



Programmed and self-organized flow of information during morphogenesis

Claudio Collinet¹ and Thomas Lecuit^{1,2}

Abstract | How the shape of embryos and organs emerges during development is a fundamental question that has fascinated scientists for centuries. Tissue dynamics arise from a small set of cell behaviours, including shape changes, cell contact remodelling, cell migration, cell division and cell extrusion. These behaviours require control over cell mechanics, namely active stresses associated with protrusive, contractile and adhesive forces, and hydrostatic pressure, as well as material properties of cells that dictate how cells respond to active stresses. In this Review, we address how cell mechanics and the associated cell behaviours are robustly organized in space and time during tissue morphogenesis. We first outline how not only gene expression and the resulting biochemical cues, but also mechanics and geometry act as sources of morphogenetic information to ultimately define the time and length scales of the cell behaviours driving morphogenesis. Next, we present two idealized modes of how this information flows — how it is read out and translated into a biological effect — during morphogenesis. The first, akin to a programme, follows deterministic rules and is hierarchical. The second follows the principles of self-organization, which rests on statistical rules characterizing the system's composition and configuration, local interactions and feedback. We discuss the contribution of these two modes to the mechanisms of four very general classes of tissue deformation, namely tissue folding and invagination, tissue flow and extension, tissue hollowing and, finally, tissue branching. Overall, we suggest a conceptual framework for understanding morphogenetic information that encapsulates genetics and biochemistry as well as mechanics and geometry as information modules, and the interplay of deterministic and self-organized mechanisms of their deployment, thereby diverging considerably from the traditional notion that shape is fully encoded and determined by genes.

The making of an embryo entails the production of billions of cells from one cell, the fertilized egg, and their organization into tissues that gradually change shape. This process, known as morphogenesis, consists of characteristic patterns of 3D deformations occurring in specific sequences. The high reproducibility of the shapes produced during embryogenesis argues that tissue remodelling is tightly controlled in space and time and that some sort of information is produced, read and interpreted by cells in the embryo to organize their behaviour. The concentration of specific biomolecules, the mechanical properties and the shape of the surrounding in which cells are located and the mechanical forces they are subjected to are a few examples of the kind of input cells interpret to define their specific behaviour. This information also ensures that tissue shape persists despite the fact that molecules and cells turn over within minutes or days. This Review aims to define the nature of this morphogenetic information and explains the modalities of its deployment during development.

Morphogenesis involves a stereotypical set of fundamental processes driven by cell mechanics that combined give rise to a multitude of tissue and organism shapes. These include: bending or invagination, which generates tissue out-of-plane deformations; tissue flow and extension, which include planar expansion of the tissue and rotational flows; hollowing, that is, the formation of internal fluid-filled lumens within a tissue; and tissue branching, which gives rise to 3D arborization. In all cases, cells change shape, divide and move with respect to one another. All these processes require mechanical forces, such as tension through contraction of actomyosin networks, cell–cell and cell–substrate adhesion, cell protrusive forces or cell growth. These active forces must be organized in space and time to correctly orient and execute these different morphogenetic processes. Thus, the primary role of the morphogenetic information is to orchestrate cellular mechanics.

The quest to identify the nature of morphogenetic information has fascinated scientists for centuries but

¹Aix-Marseille Université & CNRS, IBDM – UMR7288 & Turing Centre for Living Systems, Campus de Luminy Case 907, Marseille, France

²Collège de France, Paris, France.

✉ e-mail: thomas.lecuit@univ-amu.fr

<https://doi.org/10.1038/s41580-020-00318-6>

Box 1 | The ‘mosaic’ and the ‘regulative’ theories of development

At the end of the nineteenth century two contrasting views of development animated the discussion between embryologists. In 1888 Wilhelm Roux published a series of experiments in which he killed with a hot needle half of the 2- or 4-cell stage frog embryos and reported that these embryos grew only half of the animal³. This led him to propose his ‘mosaic’ theory of development wherein the fate of each cell was predetermined and fixed from the 2-cell embryo stage onwards. According to this theory, after a few cell divisions, the embryo is like a mosaic where each cell has a specific function and will give rise to different structures of the animal.

In contrast to this theory, Hans Driesch in 1891 separated the two blastomeres of a 2-cell stage sea urchin embryo and found that each could give rise to a complete, although smaller, embryo¹³. In line with these experiments, a few years later, in 1895, Thomas Morgan found that if instead of killing one of the two blastomeres of the 2-cell stage frog embryo (as in the case of the experiments performed by Roux), it was pipetted out, the remaining single blastomere could give rise to the entire animal, showing that the fate of cells was not fixed but rather could change according to environmental conditions. A few years later Hans Spemann showed that when a salamander embryo at the blastula stage is cut in half, if each of the halves receives part of the dorsal blastopore lip, it is able to give rise to a well-proportioned tadpole¹⁵. Altogether these experiments led to the ‘regulative’ view of development, postulating that the entire early embryo constitutes a self-differentiating morphogenetic field in which cells communicate with each other over great distances and are able to regulate each others’ choices. The mosaic and the regulative theories of development represent the ancestors of the current views whereby development is seen as deterministic or self-organized.

has evolved slowly. Key findings from the early twentieth century to the 1990s led to the emergence of the idea that morphogenetic information is encoded by genes that direct developmental processes as a hard-wired programme. Development was seen as a sequence of cellular decisions, a ‘cellular automaton’, leading to the differentiation of different cell types occurring on a developmental landscape sculpted by genes^{1,2}. Genes defined the developmental trajectories of each cell. This deterministic view has roots in Roux’s ‘mosaic’ theory of development^{3,4} (BOX 1) whereby the fate of each cell in an embryo is pre-specified very early on and follows fixed developmental trajectories. The description of stereotyped lineage trees in *Caenorhabditis elegans*^{5,6} and urochordates⁷, where genetic determinants segregate at each cellular division defining different cell populations in the progeny, consolidated this view. The idea of a genetic programme controlling development also has roots in the identification of ‘morphogens’, molecules that determine the positional information within a field of cells via their local concentration. Likewise, genes acting as ‘selectors’ interpret this positional information, transmit it to the progeny and drive morphogenesis by controlling a battery of downstream ‘realizator’ genes^{8,9}. The discovery of so-called ‘master genes’, the simple expression of which is sufficient to direct the entire genetic programme to form an organ, exemplified this view. Remarkable examples of this are *eyeless* and *shavenbaby* in *Drosophila melanogaster*^{10–12}, which direct the formation of the eye and larval denticles, respectively. Thus, a long tradition substantiated the notion that morphogenetic information is chiefly genetic in nature and operates as a deterministic programme.

However, several observations contrasted with this central idea, suggesting that development could not possibly result from simple deterministic rules. Already in the late nineteenth century Driesch and Morgan showed

that when sea urchin and amphibian embryos were cut in half, they could rewire development to regenerate the missing part^{4,13–15}. They indicated that during development cells could interact with each other and their environment and adopt a particular fate in a manner that is not predetermined. Similarly, the seminal grafting experiments in *Hydra*¹⁶ and amphibian eggs¹⁷ showed that certain groups of cells could stimulate the fate of neighbours present in a so-called competent state. Thus, development must also result from local cell–cell interactions occurring within the embryo in a self-organized manner and proceed by selection of a few viable dynamical cellular states. This so called regulatory view of development (BOX 1) contrasted with the mosaic theory of Roux in the nineteenth century. As we will see, both deterministic programmes and self-organization underlie the different aspects of morphogenesis^{18–20}.

In this Review we consider a concept of morphogenetic information that encapsulates not only genetic and biochemical activities but also mechanics and the geometry of cells and tissues. We delineate two idealized modalities of morphogenetic information flow (broadly meaning the mechanisms through which morphogenetic signals are read out and translated into a biological effect): one in which morphogenetic processes are specified and executed deterministically like a programme, and the other, in which the emergence of tissue shape rests on stochastic local interactions and feedback between parameters that characterize the system composition and configuration following the principles of self-organization. We then discuss how these two modes of information flow manifest in four broad classes of tissue deformation, namely invagination, extension, hollowing and branching.

Nature of morphogenetic information

Changing tissue shape requires control over cell shape (governed by contractile cellular machineries and cell adhesion), cell movement, cell growth and division as well as cell death. These cell behaviours may be confined to specific regions of tissues, oriented along a given axis, and temporally organized in a sequence or a cycle. Biochemistry, mechanics and geometry are three different modules of the morphogenetic information that defines the time and length scales of the molecular, cellular and tissue level processes driving tissue shape changes. The way information flows to produce biological effects defines whether morphogenesis is executed like a programme or is self-organized.

Mechano-chemical and geometrical inputs define time and length scales. Morphogenesis entails that molecular interactions acting at the nanometre scale propagate their activities over many orders of magnitude to specify macroscopic patterns. To this end, length and timescales are specified within biological structures such as cells or tissues to organize molecular processes within cells, and to drive specific cell behaviours within tissues and embryos. Biochemical interactions can define such length and timescales (FIG. 1a). The rates of chemical reactions tune how quickly specific molecules are produced or degraded, thus regulating their local concentration.

Denticles

Small cuticular bristles on the ventral side of *Drosophila melanogaster* larvae that are used for locomotion.

Strain

A measure of deformation of an object with respect to a reference length upon application of a mechanical stress. This is a dimensionless parameter

When the production of molecular species is coupled to their diffusion, striking spatial-temporal molecular patterns can emerge. Reaction-diffusion systems such as Turing instabilities²¹ produce patterns with length scales that depend on the details of activator-inhibitor interactions²² (BOX 2). Excitable systems manifest characteristic temporal dynamics, in which, for instance, trigger wave velocities depend on diffusion and positive feedback timescales²³. Concentration gradients of molecules where the local concentration depends on the production-degradation rates and on the diffusion/transport

constants²⁴, define time and length scales of morphogenetic fields. The emergent biochemical patterns are read and interpreted by cells via cell signalling and direct a sequence of downstream cellular decisions. For instance, the concentration-dependent activity of morphogens transforms a homogeneous field of cells into discrete regions of defined length, each with its own morphogenetic and differentiation programmes driven by the induction of specific changes in gene expression^{25,26}. As another example, Turing instabilities control palatal ridges²⁷ and digit number in growing limbs²⁸ in the

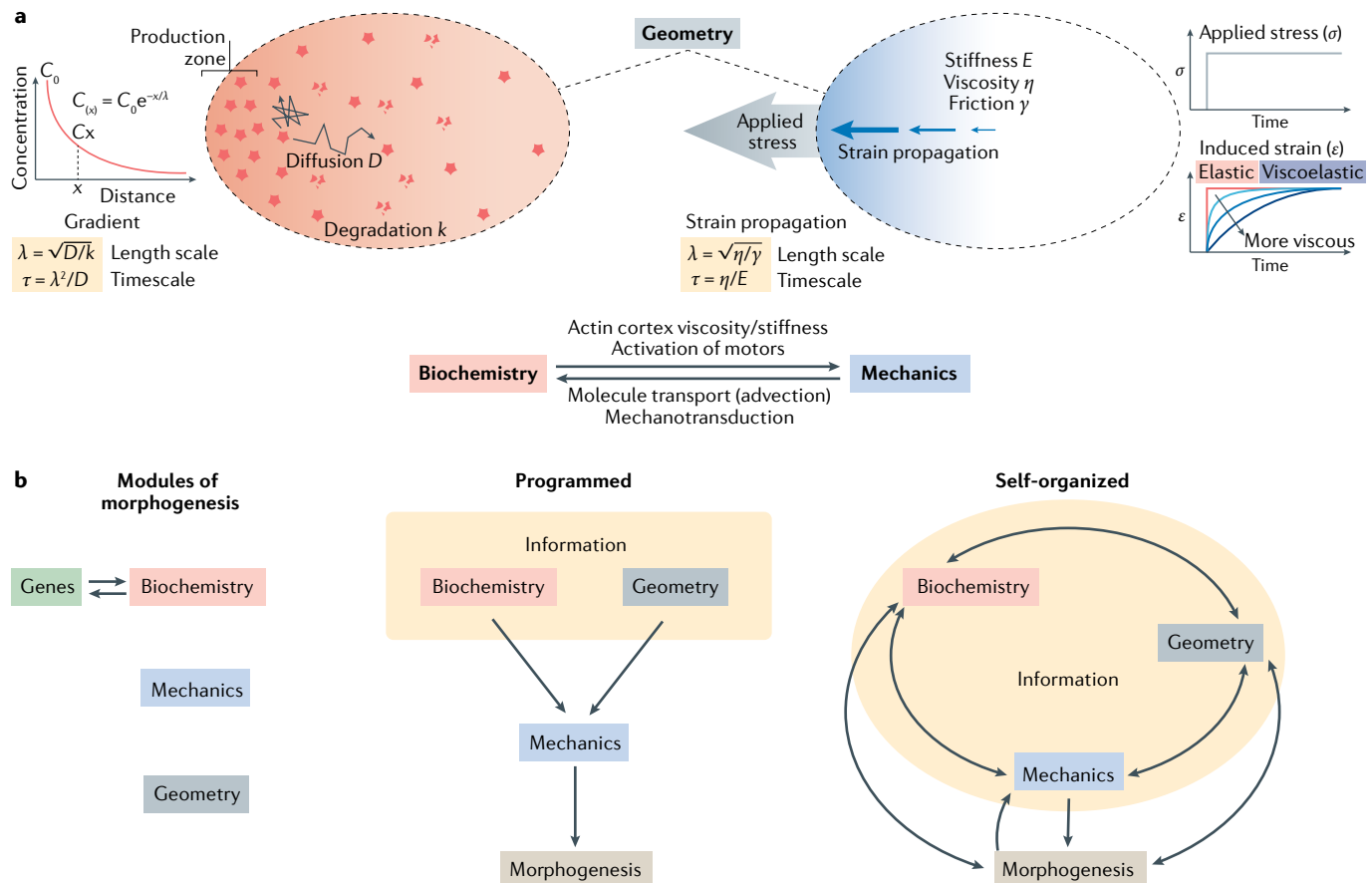


Fig. 1 | Programme versus self-organization in the flow of morphogenetic information. **a** | Length and timescales of morphogenetic information can be defined by biochemical (in red on the left) or mechanical (in blue on the right) interactions occurring within the given geometry of the tissue (in grey). On the left: the constant of effective diffusion (D) of a molecular species (red star) from a spatially restricted production zone and its rate of degradation (k) define the local concentration and thus the length scale (λ) and timescale (τ) of the cellular and tissue level processes driving shape changes. These length and timescales can be quantitatively estimated by measuring D and k (equations in the yellow quadrant). The graph on the left illustrates the spatial decay of the concentration of a molecular species following an exponential decay with length scale λ . On the right: the propagation of deformation due to an applied stress can define the length scale (λ) and timescale (τ) of morphogenetic events in a tissue. Strain propagation depends on the elastic modulus (stiffness) E , the viscosity η and the friction coefficient γ . The length (λ) and timescales (τ) are defined quantitatively as in the yellow quadrant at the bottom left. The graph illustrates how the viscosity of a material impacts on the timescale of deformation following an applied stress. A fully elastic material has a coefficient of viscosity equal to 0 and never dissipates the elastic energy due to the applied stresses (that is, it can return to their initial configuration when the stress is released) while

a viscoelastic material dissipates the elastic energy (that is, it cannot return to the initial configuration upon stress release) when the stress is applied for long enough beyond a certain timescale. The applied stress is indicated by σ and the induced strain by ϵ . Of note, biochemical interactions and cell and tissue mechanics can regulate each other. For instance, biochemical signalling can regulate the stiffness/viscosity of the actin cortex or may activate force-generating molecular motors. Mechanics can regulate local protein concentrations by advection or elicit biochemical signalling via mechanotransduction. **b** | Idealized information flows illustrating how morphogenesis could be executed as a programme (middle) or emerge in a self-organized fashion (right). Biochemistry, mechanics and geometry are the key modules of morphogenesis (as illustrated in part **a**). In programmed morphogenesis the information is fully encapsulated in the initial patterning (that is, biochemistry) and geometry of the tissue. This determines fully the execution of cell and tissue mechanical operations and the final outcome of morphogenesis. The strict hierarchy and the unidirectional flow of information are represented by single-headed arrows. In the case of self-organized morphogenesis biochemistry, mechanics and geometry can regulate each other as a result of multiple feedbacks and thus the information emerges and is continuously modulated during the morphogenetic process.

Box 2 | Length scales in mechano-chemical instabilities

Patterns emerge over a range of scales, from molecular mixtures to cellular populations in developing organisms. Irrespective of specific molecular mechanisms, Turing introduced a framework to explain how such patterns arise and symmetries are broken. In his seminal article²¹, Turing explored how reaction and diffusion in chemical systems create heterogeneity, through local activation and long-range inhibition (see the figure, left top and bottom panels). In this framework, an activator of a particular reaction or process stimulates its own production as well as that of its own inhibitor. If the inhibitor has a greater diffusion constant than the activator, the latter can accumulate locally, and a stable spatial pattern of its concentration emerges from a uniform initial state by amplification of small fluctuations in concentrations of the activator and inhibitor. The length scale of the pattern depends on details of the reaction–diffusion, such as differential diffusivity. Digit number and plate ridges in the mouse are proposed to reflect chemical Turing instabilities^{27,28,208}. Analogous instabilities arise by controlling mechanical parameters rather than molecular diffusion. For instance, the pattern of feather buds results from self-organized aggregation of mesenchymal cells migrating on an elastic substratum (see the figure, middle top and bottom panels). In this case, a local positive feedback couples an active stress associated with cell traction and an elastic stress due to extracellular matrix (ECM) deformation. The elastic resistance of the matrix is akin to a long-range inhibition and tunes the spacing between cell clusters^{34,35}. Actomyosin networks also produce contractile instabilities *in vitro* and *in vivo*. In the *Drosophila melanogaster* trachea, rings of actin emerge from motor-driven actin flow, resisted by friction within cells³⁶ (see the figure, right top and bottom panels). Flow-driven advection of actin and myosin introduces a positive feedback on actomyosin contraction. Frictional forces inhibit flow and reduce the length scale between actin rings. Thus, mechano-chemical systems control the length scale of patterns in molecular and cellular systems.

Reaction–diffusion systems

Mathematical models describing the change in space and time of the concentration of one or more chemical substances. They typically consider local chemical reactions producing or consuming chemical species and their diffusion.

Turing instabilities

A reaction–diffusion system in which the homogeneous equilibrium of mixed chemical substances is unstable owing to random fluctuations and differential diffusion. This gives rise to stationary wave patterns.

Excitable systems

Mechanochemical systems in which positive feedback and delayed negative feedback produce dynamical patterns of activity exhibiting bistability (a stable switch to an on or off state), pulses or oscillations. Spatial coupling mechanisms (for example, diffusion) lead to the emergence of waves of activity as illustrated in the classical example of the action potential.

Morphogenetic fields

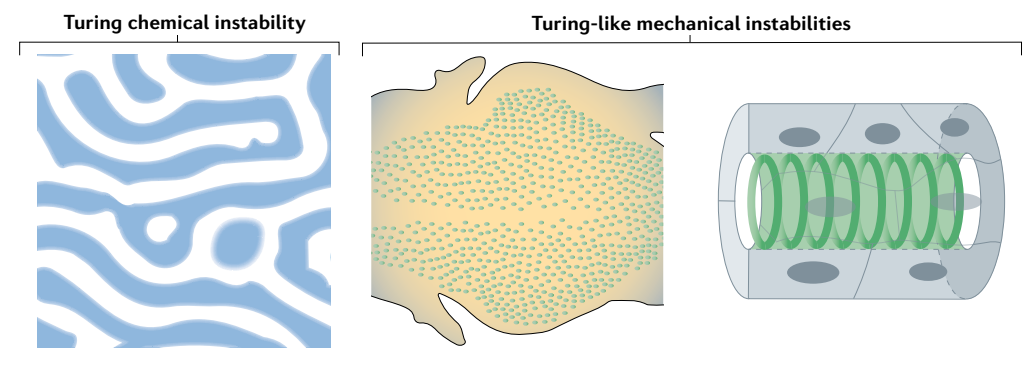
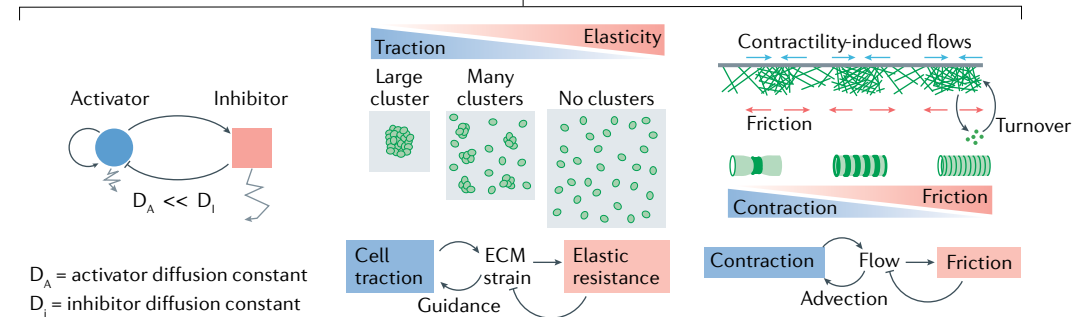
Groups of cells responding to discrete, localized biochemical signals leading to the development of specific morphological structures or organs.

Mechanical stress

A physical quantity that expresses the mechanical forces that neighbouring particles of a continuous material exert on each other. It has the dimension of force per surface area (N m^{-2}) or pressure (Pa).

Viscous response

Deformation of a viscous element, which resists shear flow and strain linearly with time when a stress is applied.

**Local positive feedback — long-range inhibition**

mouse. Kinetics of transcription factor activation and/or accumulation can be used to generate temporal patterns of gene expression defining when and in which sequence specific morphogenetic operations occur, as illustrated in the vertebrate segmentation clock²⁹. Finally, directional information (for example, apical to basal, anterior to posterior) can come from the polarized accumulation of specific molecules in cells. Thus, scalar information (that is, the concentration of a molecule) can produce vectorial or tensorial information, namely the orientation of cell polarity, cell shape and dynamics.

Mechanical parameters such as tissue elasticity, viscosity and friction can also specify time and length scales of morphogenetic processes (FIG. 1a). For instance, the length scale of stress propagation, the so-called hydrodynamic length, depends on the relative contribution

of viscosity and friction within a cell³⁰ or a tissue. Viscosity can also define rates of deformation upon a given mechanical stress. The ratio between the viscous modulus and elastic modulus defines the Maxwell time, that is, the time above which deformations become irreversible, typical of a viscous response³¹. Mechanics can thus direct morphogenesis in a manner similar to biochemical information. For instance, dissipation of a localized stress by friction can generate gradients of stress similar to those better known for biochemical gradients of morphogens^{32,33}. Turing-like mechanical instabilities produce cellular patterns with length scales governed by the elastic resistance of the extracellular matrix to active stresses produced by motile cells as in the case of feather bud morphogenesis^{34,35} (BOX 2). Subcellular patterns of actin assembly also emerge from

the frictional resistance to actomyosin active hydrodynamic flows³⁶ (BOX 2). The length scales are tuned by the competition between a local positive mechanical feedback and a long-range inhibition (elasticity or friction). Furthermore, mechanosensation and mechanotransduction, by specialized cellular structures such as tight and adherens junctions^{37–40} as well as focal adhesions^{39,41,42}, can elicit specific signalling driving cell behaviours⁴³. Mechanical stresses can also vary in direction (for example, isotropic or anisotropic) or in nature (for example, tensile versus shear stresses) and thus can define the type and direction of cell and tissue deformations.

Thus, morphogenetic information is both chemical and mechanical and often exhibits hallmarks of mechano-chemical coupling^{19,44}. Thus, the interplay between biochemical reactions and mechanical processes eventually defines length and timescales for morphogenetic processes. For instance, positive and negative regulators of mechanics (for example, Rho pathway components) may be advected^{45,46} or recruited⁴⁷ by contractile actin filament networks (FIG. 1a), or a specific cell signalling pathway may be elicited through mechanotransduction.

Both biochemical and mechanical information operate in an environment that is defined by the geometrical configuration of the tissue, namely its dimensionality, size and curvature. These factors constrain how biochemical and mechanical activities are deployed in space and time. Geometry enables non-local coupling between different parts of a cell, tissue or embryo, and defines boundary conditions dictating how stress is distributed within a tissue³³. This has important consequences in the way mechano-chemical information affects the cellular processes that drive morphogenesis. For instance, polarized cell intercalation drives linear tissue extension or rotation depending on whether tissue boundaries and the axis of polarization are linear or circular. As another example, tissue conformation changes modulate the local concentration of morphogens^{18,48,49}. Thus, tissue geometry contains information that complements and interacts with mechano-chemical information during morphogenesis.

Programme versus self-organization in morphogenetic information flow. We present two idealized modes of morphogenetic information flow: one in which morphogenesis is carried out as a predetermined programme and another in which it is self-organized (FIG. 1b). These modes represent two ends of a continuum spectrum that often coexist in a given process.

In programmed morphogenesis information is prescribed by a set of initial conditions (for example, genetic/biochemical patterning and/or initial geometry) and determines fully the mechanical behaviour of cells (for example, distribution of active stresses), the number, amplitude, location and time of morphogenetic processes and the final shape. Thus, the initial information, which is visible as an inherited pre-pattern such as a chemical gradient, foretells the final outcome of the morphogenetic process. A strict hierarchy, a unidirectional flow of information and deterministic rules are characteristic features of a morphogenetic programme. The interactions between the players of morphogenesis can be direct or indirect, that is, mediated by

intermediate layers of controllers and effectors, organized in functional units (for example, cell division or cell contraction). For instance, patterning cues might control the expression of a master gene (for example, *shavenbaby*), the activation of intermediate regulators and effector molecules (for example, actin nucleators or cuticle synthesis enzymes) to determine a specific cell behaviour (for example, denticle formation)¹².

By contrast, in self-organized morphogenesis the initial tissue state is homogeneous and does not foretell the final outcome of morphogenesis. Shapes emerge from an apparently disordered state associated with stochastic fluctuations. Amplification of local fluctuations in the parameters that characterize the system composition and configuration through feedback and spatial coupling let the system evolve towards an organized steady state. Self-organization is characterized by the absence of a hierarchy between information modules and by multidirectional flows of information. Biochemistry, mechanics and global geometry influence each other, forming constantly updated information that drives tissue shape changes. Thus, mechanics and the evolving shape (geometry) of the tissue are part of the information itself and not just under its control. This is exemplified by the processes of morphogen gradient bending in the chick intestinal villi⁴⁹ or luminal signalling in the zebrafish migrating lateral line primordium⁴⁸ where tissue mechanics and morphogenesis remodel morphogen gradients and tissue patterning. The bending of the intestinal epithelium during villification concentrates an otherwise uniform distribution of the morphogen Sonic Hedgehog (Shh) at the tip of villi, thus restricting the specification of intestinal progenitors to the crypts⁴⁹. In the zebrafish lateral line, rosette formation due to contractility-dependent apical constriction restricts a source of the secreted biochemical signal FGF into a shared microlumen where FGF concentrates and activates downstream target genes⁴⁸.

Tissue folding and invagination

Curving and bending tissues lead either to the formation of stable folds or to complete tissue invagination. Embryonic tissues invaginate to produce independent tissues such as the neurectoderm, which gives rise to the neural tube, the mesoderm, to muscle tissues, and the endoderm, to many internal organs (for example, the gut). Adult organs are also often folded (for example, the brain). Tissue-intrinsic active stresses, such as actomyosin contractions or tissue growth, together with external stresses stemming from the geometrical configuration of the tissue and its boundaries, drive bending and folding. From the point of view of morphogenetic information flow, folding and invagination may occur at very specific locations and may be accomplished through defined steps determined genetically. However, folding may also display features of self-organization, that is, arise at locations without a strictly defined cue.

Contractility-driven invaginations. Tight control over tissue bending and invagination occurs during gastrulation as it is essential that the different germ layers are properly configured in 3D. A general mechanism of

Boundary conditions

Constraints defining the limits of a system. In the case of morphogenesis these are typically the physical boundary of a tissue or an embryo.

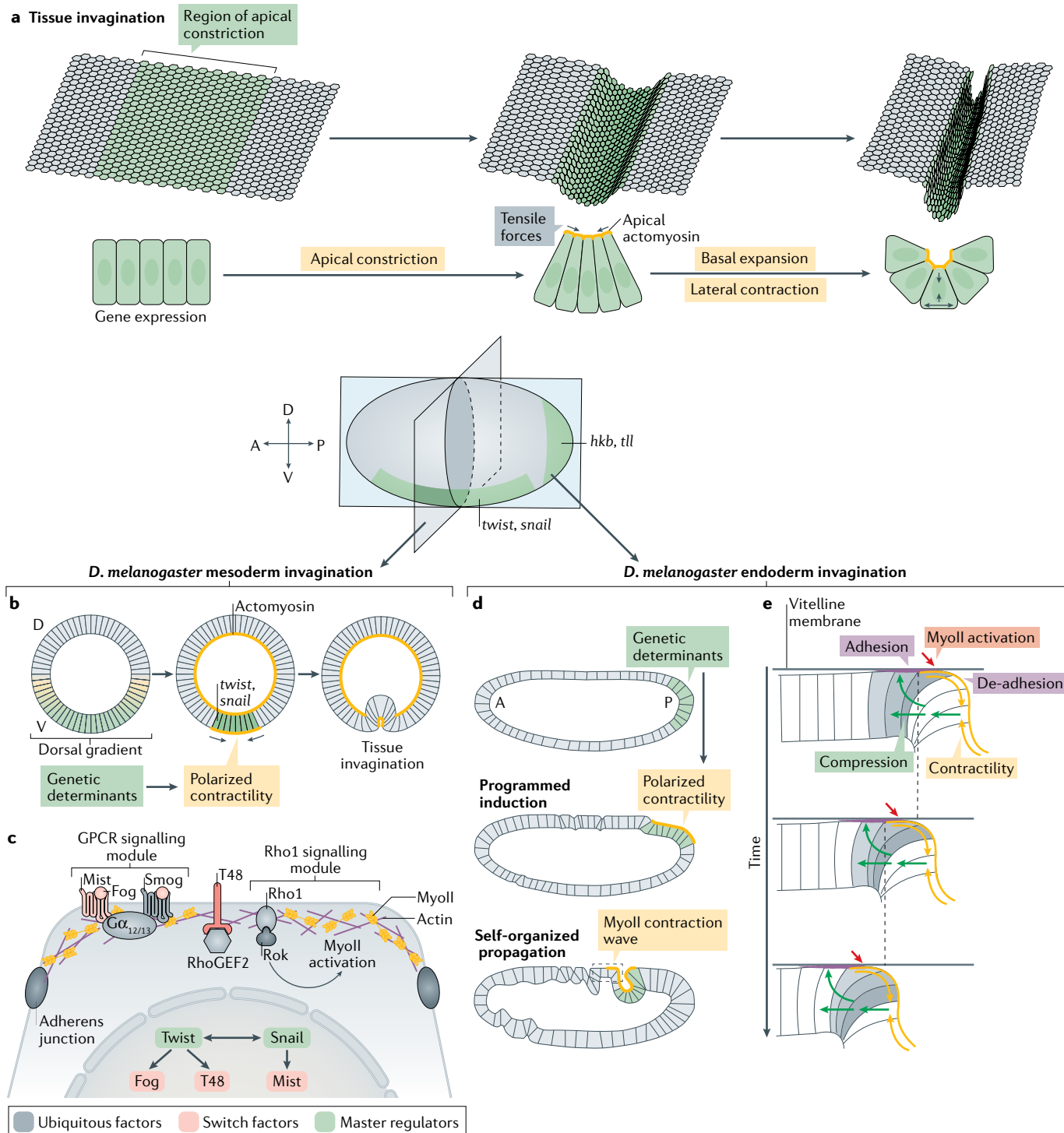
Lateral line

A sensory system comprising clusters of mechanosensory epithelial cells (neuromasts) arranged as rosettes with their apical surface facing a shared lumen. The lateral line is initially established by a migratory group of cells, called a primordium, that deposits neuromasts at stereotyped locations along the surface of the fish.

gastrulation involves the constriction of the apical surface of the embryonic epithelial cells followed by contraction of their lateral surfaces and basal expansion (FIG. 2a). Controlling the geometry of the tissue domain where cells change their 3D shape and the timing of these changes determine precisely where and when invaginations occur in the embryo. These aspects are controlled by genetic patterning and typically follow the principles of a morphogenetic programme.

The mechanics of contractility-driven tissue invaginations have been thoroughly studied in *D. melanogaster*

where the invagination of the ventral cells that form the mesoderm illustrates how cell contractions drive invaginations as a programme^{18,50,51}. Briefly, along the ventral side of the fly embryo a band of cells forms a furrow and internalizes^{52,53} (FIG. 2b). Pulsed contractions of an actomyosin network at the medio-apical cortex of mesodermal cells drive their apical constriction⁵⁴ and cell lengthening along their apico-basal axis⁵⁵ in discrete steps^{50,51,54}. Then, cells expand their basal surface via local downregulation of actomyosin contractility⁵⁶, and the persisting lateral contractility facilitates invagination⁵⁷.



Mena/VASP

Members of the VASP (vasodilator-stimulated phosphoprotein) family of proteins regulating the dynamics of the cortical actin cytoskeleton as downstream effectors of the Rho-family small G proteins Rac and Cdc42.

Shroom family proteins

Family of proteins characterized by a specific arrangement of an N-terminal PDZ domain, a central ASD1 (Apx/Shrm Domain 1) motif and a C-terminal ASD2 motif. ASD1 is required for targeting actin, while ASD2 is capable of eliciting an actomyosin constriction event.

Similarly, during endoderm invagination in the urochordate *Ciona intestinalis*, cells first induce apical constriction by apical activation of MyoII, followed by lateral cell shortening also requiring MyoII contractility⁵⁸. Thus, polarized regulation of apical, lateral and basal actomyosin contractions underlies stepwise cell deformation during tissue invagination. The extent and sequence of spatially controlled cell contractions determine the complex morphology of the invagination⁵⁸.

Spatial and temporal control of actomyosin contractility follows the principles of a genetic programme in the *D. melanogaster* mesoderm. Here, the small GTPase Rho1 (homologue of RhoA in mammals), through activation of the kinase Rok (called ROCK in mammals), controls MyoII contractility^{59,60} (FIG. 2c). Rho1 activation is necessary and sufficient to elicit apical constriction and tissue invagination⁶¹. The spatial and temporal pattern of Rho1 activation defines the pattern of tissue invagination⁶¹. In the *D. melanogaster* embryo the expression of the transcription factors Twist and Snail, which in turn depends on the dorsal–ventral gradient of the transcription factor Dorsal⁶², patterns Rho1 activation and MyoII contractility (FIG. 2b,c). Twist and Snail drive the expression of the G protein-coupled receptor (GPCR) Mist⁶³, its secreted ligand Folded gastrulation (Fog)⁶⁴ and the transmembrane protein T48 (REF.⁶⁵), which boosts recruitment of Rho1 guanine nucleotide-exchange factor (RhoGEF2) to the apical surface, where it activates Rho1. Thus, *twist* and *snail* form a ‘genetic switch’ and drive tissue invagination as a programme, whereby they

receive input from developmental patterning cues and control the cellular effectors of the programme.

Similarly, in *C. elegans*, contractions of a medio-apical actomyosin network drive apical constriction and invagination of the two endoderm precursor cells^{66,67}. The specific and polarized activation of MyoII in these cells is controlled by the Wnt–Frizzled signalling pathway⁶⁶ and two endoderm specific transcription factors, END-1 and END-3 (REF.⁶⁸). In vertebrates, apical constriction drives tissue bending during the neural tube closure in several organisms^{69,70}, gut morphogenesis in *Xenopus laevis*⁷¹ and the eye lens placode invagination in the mouse^{72,73}. The conserved RhoA–ROCK–MyoII module, together with other actin regulators (Mena/VASP), tune the contractile forces driving apical constriction. The proper spatial and temporal activation of this module is controlled by genetic patterning through tissue-specific expression of the Shroom family proteins^{71,72,74}. These proteins bind apical cell–cell junctions^{75,76} and direct MyoII activation through their direct binding to ROCK.

Altogether, these findings highlight how tissue invaginations can be directed by tissue-specific genetic programmes that determine the spatial and temporal patterns of MyoII activation and ultimately subcellular polarization of contractile forces. Nevertheless, this conceptual framework fails to explain all features of contractility-driven invaginations, suggesting that invagination is also driven by self-organized phenomena. First, the pulsed actomyosin contractions driving invagination, which are a common feature observed in many developmental contexts^{67,77–81}, are not specified genetically but instead depend on self-organizing properties of actomyosin networks due to their association with upstream regulators of MyoII contractility^{45,47,59,60}. Second, tissue-level properties such as spatial coordination of contractions⁸² and the robustness of the invagination⁸³ are emergent properties of the cell collective in which cells are connected by a supracellular actomyosin mesh. Third, the emergent mechanical properties of this supracellular actomyosin network can in some cells override the genetic programme driving apical constriction in their neighbours⁸⁴.

Self-organizational features of contractility-driven invaginations can also manifest in the dynamics of the invagination process, that is, how the tissue reaches its final shape from a specified initial pattern. In some cases, the final shape greatly diverges and cannot be predicted from the pattern of the triggering input. This was shown using modelled epithelia⁸⁵ where tissue invaginations of different shapes arise by apical constriction in a self-organized fashion using a single cell as a trigger for inducing invagination. The model, based on an excitable apical cortex, which posits that cell contraction is induced only upon cell stretching above a given threshold, predicted waves of apical constriction initiating from such a single contracting ‘triggering’ cell and spreading through the tissue to drive tissue-wide shape change⁸⁵. Tuning of mechanical parameters input into this model produced a variety of configurations observed in invaginating tissues *in vivo*. Similar induction and self-propagation of a wave of MyoII contractility driving cell invagination occurs during *D. melanogaster*

◀ Fig. 2 | Polarized contractility drives tissue bending and invagination.

a | Tissue bending and deep invagination is driven by cell apical constriction followed by shortening of the lateral surfaces and widening of the cell basal sides. Programmed genetic patterning defines the region of bending or invagination by inducing the expression of genes (labelled in green), protein products of which — via downstream biochemical signalling — activate polarized contractility in cells (in yellow). This in turn drives cell apical constriction and basal expansion. b,c | Mesoderm invagination in the *Drosophila melanogaster* embryo is an example of programmed contractility-driven invagination. Part b shows the transverse section of the embryo illustrating the invagination of the mesoderm. The dorsal (D)–ventral (V) gradient of nuclear protein Dorsal, acting like a morphogen, defines the domain of expression of *twist* and *snail* and in turn the domain of polarized actomyosin contractility driving tissue invagination. Part c gives a detailed illustration of the molecular pathway involved in the activation of polarized apical contractility. The transcription factors *Twist* and *Snail* act like master regulators that drive the expression of genes encoding three switch factors: the ligand Fog, the G protein-coupled receptor (GPCR) Mist and the molecular scaffold T48 (Smog, which is another receptor for Fog, is a ubiquitous factor and is not under the control of *twist*/*snail*). These factors activate the ubiquitous Rho signalling module and direct myosin II (MyoII) activation on the apical side of the cell. d,e | Posterior endoderm invagination in the *D. melanogaster* embryo is an example of cooperation between programme and self-organization to drive morphogenesis. Part d shows the sagittal section of the embryo, illustrating the invagination of the posterior endoderm. The expression of terminal patterning genes *hkb* and *tll* (in green) defines the region of initial actomyosin contraction (in yellow) and thus the site of initial tissue invagination. This is followed by a wave-like propagation of actomyosin contractility beyond the region specified by the patterning genes. The MyoII wave propagates by a self-organized mechanism. Part e gives a detailed illustration of the self-organized propagation of MyoII contractility. In the posterior invaginated part of the tissue and in the cell at the boundary of the furrow, actomyosin is anchored to the vitelline membrane through integrin-mediated adhesion. This leads to cell detachment and invagination upon MyoII activation and contraction (red arrow), and the resulting compression lifts more anterior cells, inducing their adhesion to the vitelline membrane. This shifts the adhesion region more anteriorly. Then, MyoII contractility is activated in a new cell at the boundary of the furrow, reiterating the cycle. A, anterior; P, posterior.

endoderm morphogenesis⁴³ (FIG. 2d,e). An initial phase of MyoII activation, apical constriction and tissue invagination is triggered in a spatially defined region at the embryo posterior. This initial phase is controlled by a genetic programme similar to that of the mesoderm morphogenesis, whereby the expression and secretion of the ‘switch factor’ Fog, under the control of terminal patterning⁶⁴, define the region of initial invagination and trigger MyoII activation. Subsequently, MyoII activation and cell invagination propagate anteriorly, driving the movements of the endoderm towards the embryo anterior. Importantly, this contractility-based morphogenetic wave does not depend on a wave of gene transcription or on the regulated diffusion/transport of secreted signals such as Fog activating MyoII. Instead, the wave is controlled mechano-chemically by self-sustained repeated cycles of cell deformation involving adhesion of endoderm cells to the overlaying vitelline membrane, which forms a substratum to direct tissue movements and activate MyoII through integrin-dependent mechano-chemical signalling⁴³. Thus, dynamic patterns of tissue invagination can arise from the interplay between a genetic programme that works as a trigger and self-organized mechano-chemical propagation of cell contractility.

Folding by growth-driven mechanical instabilities. Some tissues consist of many folds organized in complex patterns, such as convolutions in the brain and loops and villosities in the gut. These folds arise in sheet- or rod-like tissues owing to mechanical instabilities associated with tissue growth. An elastic material put under compressive forces folds to relax stresses above a certain threshold. Likewise, the planar growth of a tissue generates compressive stresses when the increase in tissue volume is constrained, for instance, when the neighbouring tissues do not grow as quickly (FIG. 3a). Notably, in the absence of other cues, such as molecules eliciting cell contraction, the final pattern is not strictly determined but emerges in a self-organized fashion, in that the position and amplitude of folds and loops follow stochastic rules. This typically occurs during brain folding in gyrencephalic species^{86,87} and vertebrate gut morphogenesis^{88,89}.

The brain cortex in vertebrates is characterized by a complex folding pattern with outward (gyri) and inward curvatures (sulci) (FIG. 3b). In the mature cortex these folds are evenly spaced. Brain circumvolutions form progressively on an initially morphologically smooth tissue surface^{90,91} starting with the emergence of few primary sulci at stereotyped locations^{92,93}. Then, other folds form with a lower degree of stereotypy⁹⁰. Across different species, the extent of cortical folding scales as a function of cortical surface area and its thickness in a manner similar to the crumpling of paper balls⁹⁴, suggesting that brain folding may follow principles of energy minimization⁹⁴. Although several models have been proposed^{95,96}, the source of stresses associated with cortical folding appears to be a difference in tangential expansion between the external (grey matter) and internal (white matter) layers of the brain cortex. This hypothesis⁹⁷ was consistent with theoretical studies in several contexts^{98–100}, and received support from measurements of physical forces in

developing ferret brains¹⁰¹ and more recently, from experimental testing with synthetic ‘mini brains’^{102,103}. In the latter, by controlling the stiffness of 3D gels used to construct the mini brains and with computer simulations it was shown that greater swelling of the outermost layer of the synthetic organ as compared with the inner core was sufficient to produce a wrinkling pattern with smooth gyri and cusped sulci similar to that observed in brain cortices¹⁰² (FIG. 3c). Furthermore, when the size and the shape of gel and *in silico* modelled mini brains were made similar to the geometry of fetal human brains before cortical folding, the pattern of gyri and sulci was remarkably similar to that observed *in vivo*¹⁰³. In this model, the non-uniform local curvature in the smooth template determined the spatial distribution of stresses, with highest compressive stresses at sites of primary sulci formation, which were remarkably similar to the positions found in real developing human brains¹⁰³. These findings highlight how mechanical instability and the initial fetal brain geometry could generate reproducible folding patterns. However, it was proposed that additional information is necessary to control the stereotyped folding pattern of primary sulci *in vivo*. Patterned local heterogeneities in the thickness of the subventricular zone (a region of high neurogenesis in gyrencephalic species) and the proliferation of radial cortical progenitors correlate with the position of emergence of gyri and sulci^{104–106}. A transcriptomics analysis in ferret brains identified specific modules of gene expression mapping the prospective positions of primary fissures¹⁰⁷, supporting the idea that regional differences in growth might be genetically encoded. The information required to position primary fissures thus supports the existence of an underlying programme. Brain folding thus emerges from the mutual interactions between patterning (differential growth), tissue mechanics (elasticity) and tissue geometry.

Another context in which growth-driven mechanical instabilities drive morphogenesis is the development of the gut, which undergoes looping and villification as it extends. Throughout development, the growing gut tube is attached to the dorsal mesentery, a type of membrane connecting the body to the gut tube along its entire length (FIG. 3d). Upon physical separation from one another these two tissues recoil: the tube unwinds and the dorsal mesentery shrinks, indicating that the former is compressed while the latter stretched¹⁰⁸. In their relaxed state, the two tissues have different sizes reflecting their different growth. Thus, gut looping results from buckling to relax the stress accumulating when the tissues are physically attached to one another and grow at different rates¹⁰⁸ (FIG. 3e). BMP morphogen signalling, present in a dorsal to ventral gradient from the dorsal mesentery to the mesenchyme of the gut tube¹⁰⁹, tunes the extent of differential growth and in consequence the degree of gut looping¹¹⁰, but the specific position of loops emerges stochastically. Thus, the degree of looping can be seen as encoded in a programme but the looping pattern is self-organized.

In many species the gut undergoes villification, which transforms its luminal surface from flat to convoluted with the emergence of numerous inward protrusions such as ridges, zig-zags, honeycombs and villi. The hypothesis that these structures might arise from the constrained

Vitelline membrane

Structure surrounding the outer surface of blastoderm cells in embryos of several animals including birds and insects.

growth of inner layers by outer contractile muscle cells was formulated long ago¹¹¹ and recently tested^{99,112}. In the chick, this process is well characterized and occurs in discrete steps: first longitudinal ridges form; then they fold in a zig-zag pattern and finally villi form^{111,113,114} (FIG. 3f). This tightly follows the formation of first circumferential muscles, followed by the emergence of separate layers of

longitudinal muscles. These muscle layers mechanically constrain the growth of the internal epithelial and mesenchymal layers: circumferential muscle contraction induces longitudinal ridge formation, while longitudinal muscle contraction induces lateral buckling of ridges into zigzags¹¹². The last step involves inhomogeneous growth of the intestinal epithelium where growth is confined

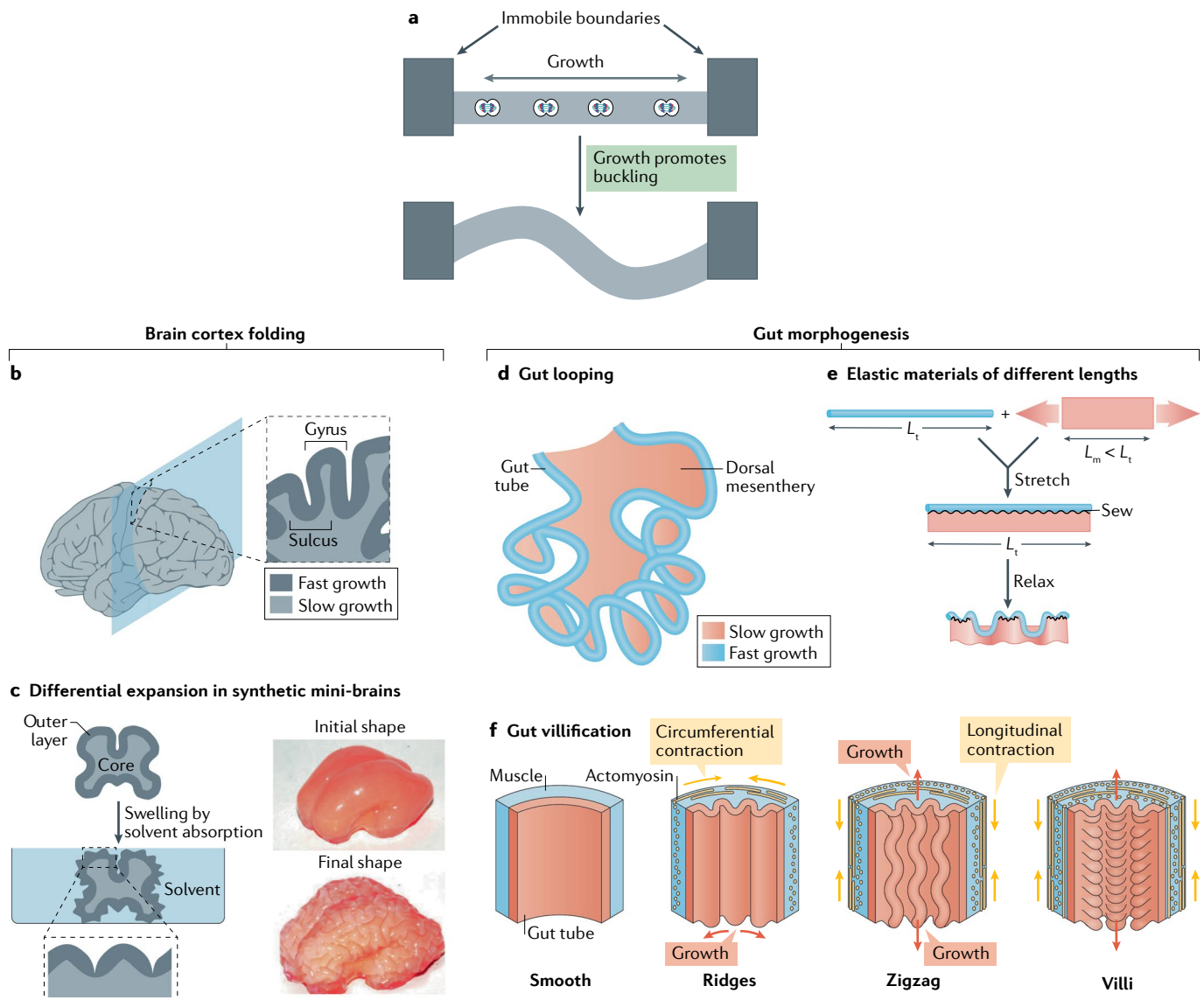


Fig. 3 | Growth-driven mechanical instabilities drive tissue folding and looping. **a** | The growth of a tissue constrained between immobile boundaries drives buckling and tissue folding. **b** | The cortex of the human brain is heavily folded in gyri and sulci. Brain folding has been proposed to emerge from a buckling instability where the fast growth of the external cortical layer (the grey matter) is constrained by the slower growth of more internal layers (the white matter). **c** | Differential growth of an outer and an inner layer in synthetic mini-brains produced from compound gels with controlled stiffness gives rise to a wrinkling pattern resembling those in brain cortices. On the left a schematic of a synthetic mini-brain composed of two different layers of PDMS gel: an outer layer that expands by swelling, which covers an inert but deformable inner layer. The stiffness of both layers can be controlled. Upon immersion in a solvent, the outer layer expands by swelling, resulting in bending of both layers, which form wrinkles and cusps similar to gyri and sulci. On the right: representative images of the gel

mini-brains before and after swelling. **d** | The looping of the small gut results from the differential growth of gut tube (blue) and of the mesentery membrane (red) that connects the body to the gut tube along its entire length. **e** | Rubber model of gut looping. Sewing a stretched rubber sheet (red) to an unstretched rubber tube along its entire length produces a looping pattern resembling those of the small intestine. **f** | The process of gut villification in chicken embryos proceeds in steps with the emergence in a sequence of ridges, followed by zig-zags and villi. The growth of the intestinal epithelium is sequentially constrained by the emergence of circumferential smooth muscles, followed by two layers of longitudinal muscles. Red arrows indicate the direction of growth constrained by muscle contraction (yellow arrows). L_m , mesentery length; L_t , tube length. Images in part **c** adapted from REF.¹⁰³, Springer Nature Limited. Schematic in part **e** adapted from REF.¹⁰⁸, Springer Nature Limited. Schematic in part **f** adapted with permission from REF.¹¹², AAAS.

to the valleys between forming villi¹¹². Interestingly, this final pattern emerges from the continually changing geometry of the tissue during the formation of villi, which bends a gradient of SHH and leads to the formation of a signalling centre at the villi tip, ultimately restricting cell proliferation to the base of villi¹⁹. Thus, in the chick, villification emerges from growth-mediated mechanical instabilities (self-organization) acting upon patterned mechanical constraints (programme).

Villification in the mouse is apparently not constrained mechanically and may depend instead on chemical (for example, Turing) instabilities^{115,116}. Self-organized patterns of BMP2 induce mesenchymal cell aggregates prior to villi formation. These aggregates cause bulging of overlying epithelial cells and initiate villi formation. Although the formation of BMP2 patterns and the ensuing aggregation of mesenchymal cells can be modelled as a Turing instability, it is conceivable that mechanics also participate in the formation of such self-organized aggregates, as postulated¹¹⁷ and subsequently tested for the morphogenesis of feather buds³⁵ (BOX 2). Mechano-chemical instabilities could therefore be a general framework for the mechanism of villification across species where similar coupling of smooth muscle layer differentiation and folding of internal layers have been observed.

Overall, brain folding and gut morphogenesis exemplify how complex shapes emerge from the interplay of stresses due to differential growth, tissue elasticity and tissue geometry where genetic programmes and self-organization cooperate to establish the final tissue pattern.

Convergence–extension

The process by which a tissue changes shape by narrowing (converging) in one direction and extending along a perpendicular axis.

Traction forces

Forces used to generate motion between a body and a tangential surface, through the use of friction or adhesion.

Contractile systems anchored to a rigid body can generate traction forces to move cells or cellular objects.

Notochord

A small flexible rod made from cells from the mesoderm and oriented head to tail in embryos of organisms of the phylum Chordata. As it is composed of stiffer tissue, it allows for skeletal support of the embryo during development.

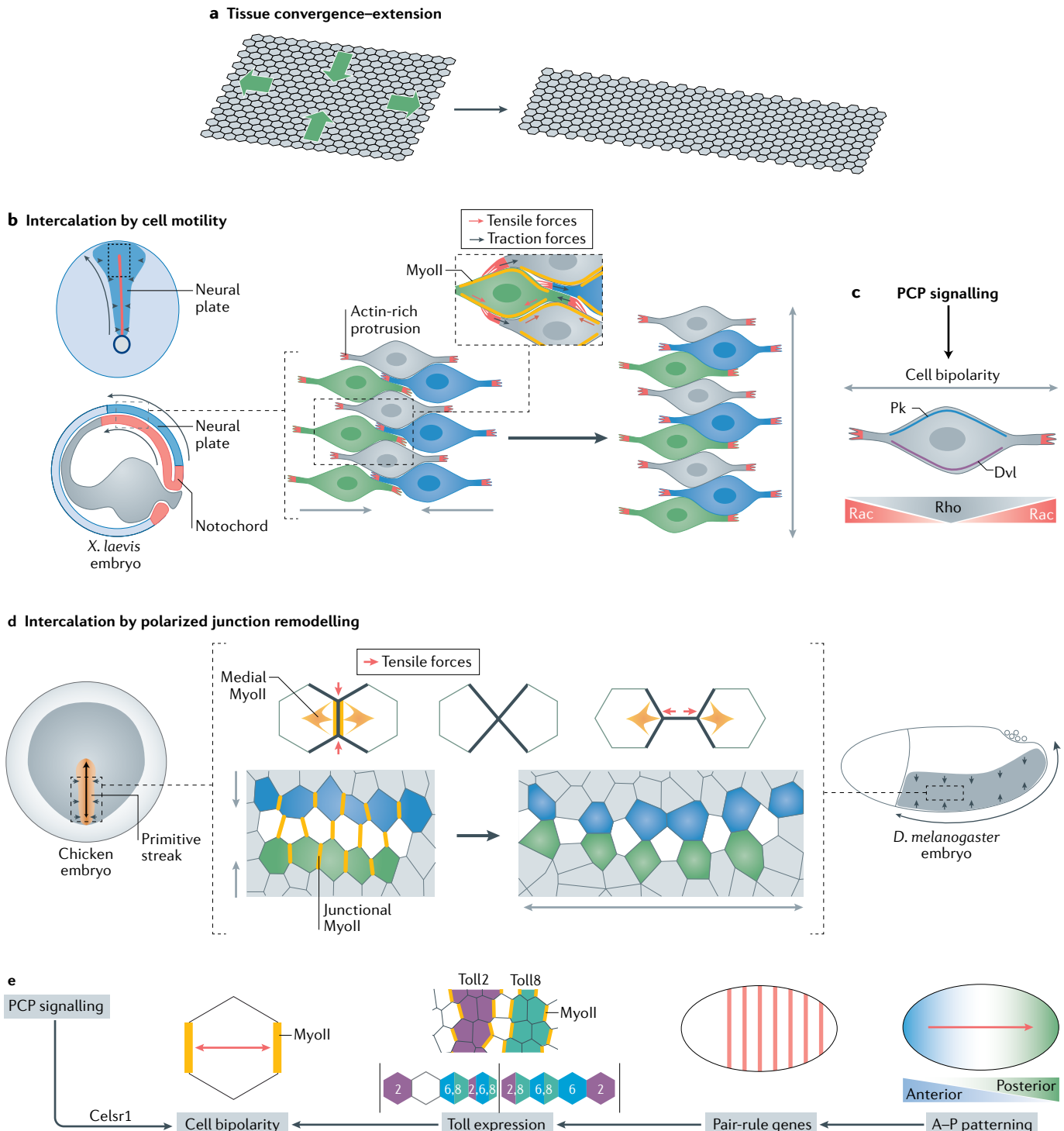
Germband

Blastoderm tissue corresponding to the ventrolateral region of the embryo in *Drosophila melanogaster* and other insects.

Fig. 4 | Tissue extension by programmed polarization of cellular active stresses. **a** | Illustration of convergence–extension movements driving tissue extension. **b** | Cell intercalation by cell motility drives convergence–extension in the *Xenopus laevis* notochord and neural plate. Cells of the notochord and of the neural plate elongate, extend actin-rich protrusions and intercalate by crawling onto one another in the medio-lateral direction extending the tissue in the antero-posterior direction. The cells exert traction forces on their neighbours by adhering with their actin-rich protrusions and contracting their medio-laterally oriented edges. **c** | Planar cell polarity (PCP) signalling controls the bipolar extension of actin-rich protrusions. The PCP proteins Pk and Dvl localize to mediolateral cell–cell contacts where Dvl activates Rho signalling. Antagonism between Rho and Rac signalling might explain the extension of actin-rich protrusions medio-laterally. **d** | Cell intercalation by cell–cell contact remodelling drives convergence–extension in the primitive streak of chicken embryos and the germband in *Drosophila melanogaster*. Planar polarized actomyosin contractility drives cell intercalation in two steps: first the shrinkage of cell contacts in the direction of tissue convergence, followed by the extension of new contacts in the direction of tissue extension. Contractions in an apico-medial and a junctional pool of myosin II (MyoII) generate the forces necessary for both junction shrinkage and the subsequent extension of newly forming junctions. **e** | The planar polarized accumulation of MyoII at junctions is controlled by the global polarity of the tissue (red unidirectional arrow). PCP signalling controls this via the Celsr1 receptor in chicken embryos. In *D. melanogaster* embryos antero-posterior patterning controls via pair-rule genes the expression of different Toll receptors (Toll2, Toll6 and Toll8) in stripes. The striped expression of Toll receptors generates a hypothetical combinatorial cell surface expression code that results in the planar polarization of MyoII at cell–cell junctions. A, anterior; P, posterior.

In the ascidian notochord, epithelial cells intercalate medio-laterally in a process that depends on the extension of polarized membrane protrusions along their apico-basal axis¹²⁷. During formation of the dorsal midline in *C. elegans*, polarized Rac-dependent membrane protrusions at the basolateral side of two rows of cells flanking the midline drive their migration and intercalation to form a single row of cells at the embryo midline^{128,129}. The polarized extension of actin-rich protrusion at the basolateral side of epithelial cells also occurs and contributes — together with remodelling of cell–cell junctions — to the formation of rosettes in the germband of *D. melanogaster*¹³⁰ and in the mouse neural plate¹³¹.

The second mode of cell intercalation is by polarized remodelling of cell–cell contacts via actomyosin contractions, whereby cells exchange neighbours while maintaining intercellular adhesion and tissue integrity (FIG. 4d). Cell intercalation in epithelial cells was first characterized in the germband in *D. melanogaster*¹³² where dorsal–ventral junctions first shrink and then new antero-posterior junctions form^{133,134}, thus extending the tissue along the antero-posterior axis. Planar polarized actomyosin contractility at cell–cell junctions^{133,134} and in the medio-apical cortex^{77,135–137} drives junction remodelling. Junctional MyoII accumulates at dorsal–ventral junctions^{133,134} and induces

**Primitive streak**

Transient structure that forms in the blastula during the early stages of avian, reptilian and mammalian embryonic development. It forms on the dorsal (back) face of the embryo, towards the caudal or posterior end.

anisotropic cortical tension^{138–141} while medial MyoII undergoes planar polarized flows that increase the speed of shrinkage of dorsal–ventral junctions^{77,135} and extend new antero-posterior junctions^{136,137}. Similar junction remodelling by actomyosin contractions drives cell intercalation in vertebrates, such as during primitive streak formation¹⁴² and neural tube closure in chick embryos^{69,143}. Remarkably, mesenchymal cells of the dorsal marginal zone in frog embryos present similarities to the epithelial cells of the *D. melanogaster* germband^{144,145}. Also here, phosphorylated MyoII

accumulates at mediolateral cell–cell contacts inducing anisotropic cortical tension¹⁴⁴, and actomyosin pulses correlate with steps of cell–cell contact shrinkage^{144,145}.

Thus, the extension of actin-rich membrane protrusion and remodelling of cell–cell contacts by actomyosin contraction are complementary strategies to produce local active forces required for cell intercalation.

The proper orientation of cell processes driving tissue extension requires that global tissue polarity is read out locally. In *D. melanogaster* embryos, the global polarity is encoded in the gradients of the anterior and

posterior determinants Bicoid and Caudal, which control the expression of pair-rule genes, resulting in their striped expression pattern. One of these pair-rule genes, *even-skipped* (*eve*), in turn controls planar polarization of MyoII¹⁴⁶ and cell intercalation¹³² (FIG. 4e). The polarization of MyoII by *eve* is mediated by the expression of three Toll receptors in a specific striped pattern repeated in each parasegment¹⁴⁷. The differential expression of

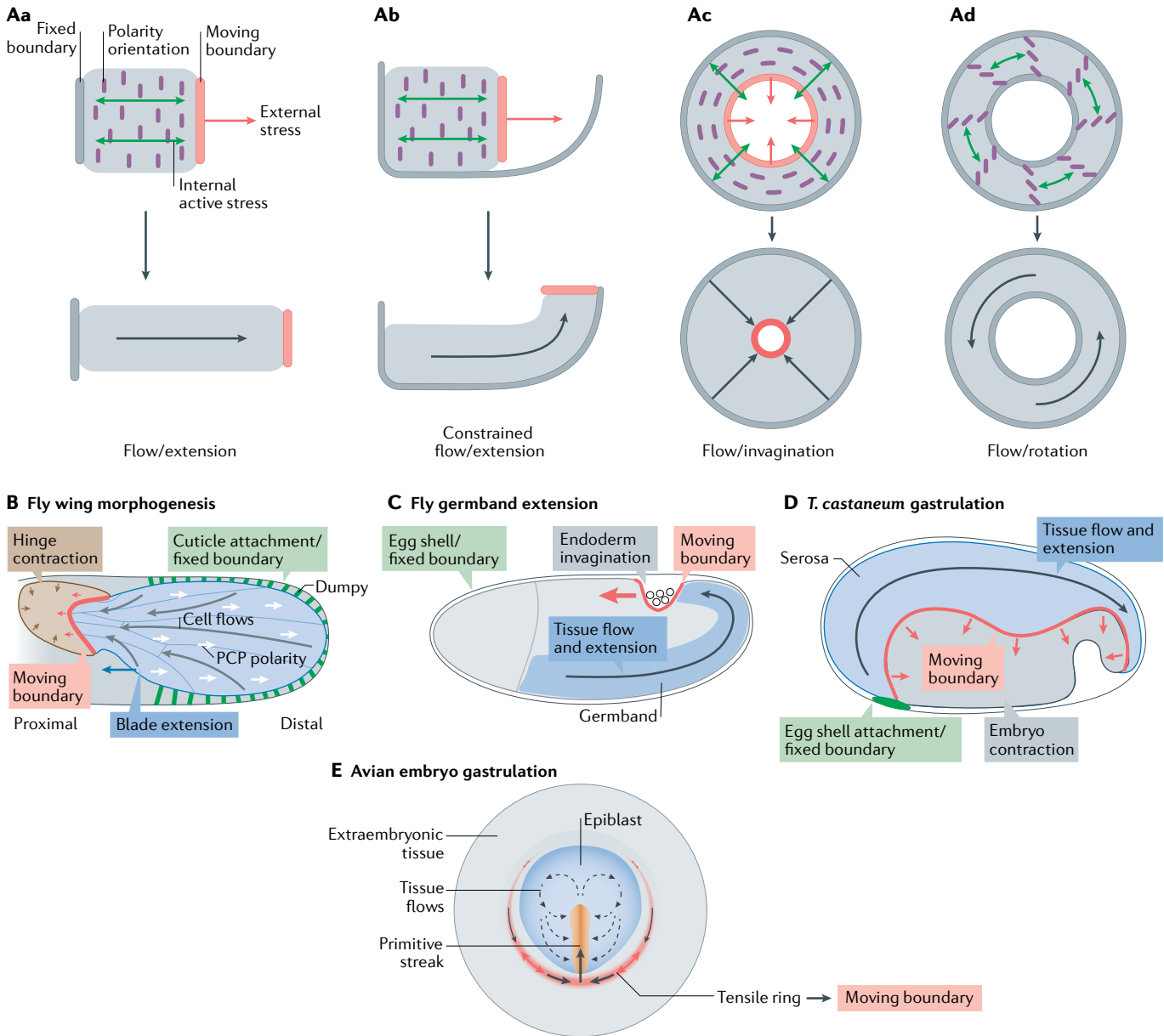


Fig. 5 | Impact of patterned boundaries and their geometry in tissue flows and extension. **A** | Impact of boundary configuration on tissue flow and extension. Tissue boundaries can be fixed (immobile) or moving (actively or passively). Both intrinsic (that is, internal stress, in green) and extrinsic (provided by actively moving boundaries, in red) stress drive tissue flow (black arrow). The direction of the flow is affected by the geometry of the fixed boundaries and by the orientation of polarity cues (in magenta) that guide accumulation of intrinsic stresses. Internal or external stresses can elongate a tissue in a given direction. The direction of the flow depends on the orientation of internal stresses or the external stress moving the active boundary (part **Aa**). The direction of the flow can be constrained by the geometry of the fixed boundary (part **Ab**). The geometry of the tissue and of the fixed boundary can generate either a centripetal flow (part **Ac**) or a rotation (part **Ad**). Tangentially oriented polarized cues orient internal stresses radially, driving centripetal flow. An extrinsic centripetal stress on the moving boundary can also contribute (part **Ac**). When the polarity cue is oriented radially, the resulting stress is a tangential shear. This drives a

rotational flow (part **Ad**). **B–E** | Examples of the impact of moving and fixed boundaries in tissue flow and extension. **B** | In the fly wing, contraction of the hinge region exerts extrinsic stresses on the wing blade orienting cell flows (grey arrows) and the orientation of planar cell polarity (PCP) proteins (white arrows). The final shape of the wing depends on the pattern of attachment of the blade region to the fixed cuticle via Dumpy. **C** | During gastrulation in fly embryos the invagination and movement of the posterior endoderm exerts pulling forces on the extending germbands (acting as a moving boundary). The egg shell provides a fixed boundary that orients the flow of the tissue. **D** | During gastrulation of *Tribolium castaneum* the serosa spreads and envelopes the contracting portion of the blastoderm, which constitutes the future embryo. The cell flows are constrained by the vitelline membrane acting as a rigid shell and the flow direction is determined by the position of attachment of the blastoderm to it. **E** | During gastrulation of the avian embryo, the large-scale tissue flows (depicted by the dashed arrows) depend on the activity of a contractile ring at the margin of the embryo, which functions as a moving boundary.

Marginal zone
Region corresponding to the equator between the two hemispheres in amphibian embryos.

Pair-rule genes
Group of genes expressed in stripes during segmentation of the embryo in arthropods. In *Drosophila* pair-rule genes form seven dorsoventrally oriented stripes disposed along the antero-posterior axis.

Toll receptors
A class of single-pass transmembrane receptors involved in patterning and immunity.

Parasegment
The fundamental unit of *Drosophila melanogaster* development, which is made up of portions of two adjacent segments along the body of the embryo.

Planar cell polarity
The coordinated polarization of a field of cells within the plane of a cell sheet. The axis of planar polarity is typically orthogonal to that of the apico-basal polarity of epithelial cells.

Septins
Cytoskeletal components that upon binding to GTP can polymerize into ordered structures such as rings and filaments, which can function as scaffolds or diffusion barriers.

Advection
The transport of a substance or physical quantity by the movement of the surrounding environment.

Dissipation timescale
Characteristic time at which the internal mechanical stress is reduced by a certain amount by viscous flow.

Bandpass filter
A filter or device that passes frequencies within a certain range and rejects frequencies outside that range.

Toll receptors between neighbouring cells along the antero-posterior axis is thought to activate MyoII at dorsal–ventral junctions^{147,148}. How Toll receptors activate MyoII at junctions is not yet clear. Tolls may polarize activity of GPCRs driving Rho1 and MyoII activation at specific junctions. Recent evidence indicates that the adhesion GPCR Cirl/Latrophilin forms a complex with Toll8 that mediates MyoII polarization¹⁴⁸. However, Toll8 and Cirl polarization are dynamically interdependent when neighbouring cells express different levels of Toll8 (REF.¹⁴⁸), indicating that although most of these mechanisms are genetically programmed, the mechanism of receptor polarization itself occurs through self-organization.

Another pathway that translates global directional information locally to cells is planar cell polarity (PCP) signalling (see REFS^{149–151} for excellent reviews). PCP signalling polarizes cells acting, among others, on Rho and Rac signalling^{118,152–155} and controls polarized cell intercalation in many mesenchymal^{156,157} and epithelial^{131,143,158} systems. In *X. laevis*, interfering with PCP signalling disrupts both the bipolar extension of actin-rich protrusions¹⁵⁷ and the contractions of medio-lateral shrinking cell–cell contacts¹⁴⁴. The precise mechanism is not yet clear. PCP proteins, which localize at medio-lateral cell–cell contacts¹⁵⁹, might polarize cells by promoting Rho signalling and MyoII activation at these contacts¹⁶⁰, thus also restricting Rac and protrusive activity medio-laterally (FIG. 4c). Septins, which act as diffusion barriers and regulate medio-lateral intercalation downstream of PCP^{144,161}, might mediate this polarized partitioning. In epithelia, PCP signalling controls directed cell intercalation in several contexts: it orients cell intercalation in the ascidian notochord primordium¹⁵⁸, it polarizes both the extension of basal protrusions and apical junctional remodelling in the mouse neural plate¹³¹ and it controls polarized MyoII activation at adherens junctions in the chick neural tube via activation of the GPCR Celsr1 (REF.¹⁴³) (FIG. 4e). These examples highlight how global spatial and directional information laid down by genetic patterning is interpreted by different planar polarity systems to control and coordinate local cell intercalation driving tissue extension.

Overall, tissue extension by cell intercalation can be seen as primarily controlled by a genetic programme. This programme view of tissue extension must be nuanced with the fact that local cell dynamics during cell intercalation follow statistical regularities rather than deterministic rules. The most striking stochastic feature is the pulsatile nature of actomyosin contractions. In the *D. melanogaster* germband, actomyosin pulses are self-organized and involve Rho1GTP oscillations, which require advection of Rho1GTP and Rok caused by MyoII contractions⁴⁵. Moreover, medio-apical pulses of actomyosin flow towards cell–cell contacts with a statistical bias in the antero-posterior direction^{77,162}, making it more likely for dorsal–ventral junctions to shrink. Last, local deformations induced by actomyosin contractions are not strictly irreversible. Only contractions that persist longer than a dissipation timescale produce permanent deformations³¹. This dissipation timescale functions as a bandpass filter for actomyosin pulses,

which are loosely controlled, thereby ensuring global persistent junction remodelling in the face of inherently fluctuating cellular dynamics. In summary, the reliance on fluctuations in cell contraction is a characteristic feature of self-organization, and thus tissue extension, at least in the *D. melanogaster* germband, involves a non-deterministic component.

Self-organization via patterned boundary conditions and external forces. Tissue flow and extension are not driven solely by polarized internal stresses. The geometry and patterning of tissue boundaries as well as extrinsic forces impact on cellular dynamics and orient tissue flows (FIG. 5). Boundary conditions can either exert mechanical feedback on cellular dynamics or simply define geometrical constraints and direct cellular flows (FIG. 5a). An example of mechanical feedback comes again from *D. melanogaster* germband extension. Here, the invaginating posterior endoderm is an actively moving tissue boundary (FIG. 5c) and exerts a posterior pulling force onto the germband^{136,163}, which orients the extension of new junctions along the antero-posterior axis between germband cells¹³⁶. This optimizes the extension process by aligning local junction extension with the global direction of tissue lengthening¹³⁶. Actively moving boundaries also organize large-scale flows associated with primitive streak formation during avian gastrulation¹⁶⁴. Here, the contraction of a supra-cellular actomyosin ring at the margin of the embryo acts as a moving boundary that drives the flows (FIG. 5e).

Feedback between extrinsic forces and intrinsic cellular processes occurs also during the morphogenesis of the fly wing. Here, a tissue-level contraction of the hinge, the part of the wing connected to the thorax, pulls and extends the wing blade along the proximo-distal axis¹⁶⁵ (FIG. 5b). This induces a pattern of cell elongation, cell rearrangements and cell divisions^{165,166} that underlies not only tissue extension but also the alignment of PCP components along the proximo-distal axis¹⁶⁵.

In addition, attachment of cells to a fixed substrate controls the orientation of tissue-level forces, ultimately defining the pattern and direction of tissue extension. In the fly wing the spatial pattern of distal attachment of epidermal cells to the overlaying cuticle by the extracellular matrix protein Dumpy directs tissue-level tension and shapes wing extension^{166,167} (FIG. 5b). Modifying the pattern of attachment has predictable consequences on the final wing shape, indicating that wing morphogenesis results from patterned tissue contraction and localized cell anchorage¹⁶⁷. Another context in which the attachment to a fixed substrate directs cellular flows is gastrulation of the red flour beetle *Tribolium castaneum*¹⁶⁸. Here, gastrulation consists of the contraction and folding of a large part (approximately two-thirds) of the epithelial blastoderm, which gives rise to the future embryo, and the spreading of the remaining third, which gives rise to the enveloping serosa. The flow of the serosa cells is unidirectional and depends on the localized attachment of the blastoderm to the overlaying vitelline membrane mediated by integrins¹⁶⁸.

Thus, tissue extension is patterned by mechanical coupling at tissue boundaries. These boundaries,

whether fixed (that is, immobile) or active (that is, moving in response to active stress), deterministically orient tissue extension and cellular flows. Yet, flow-driven morphogenesis as a whole follows principles of self-organization, given that the behaviours of the flowing cells are not individually programmed but mutually interdependent.

Of note, also the geometry of tissue boundaries contributes to orienting the flow pattern. Given that cell intercalation during tissue extension is polarized as discussed above, the boundaries — depending on their shape — may drive rectilinear, curvilinear or rotational flow as illustrated respectively in the wing, germband and male genitalia of *D. melanogaster*¹⁶⁹ (FIG. 5a). Thus, tissue boundaries carry both mechanical and geometrical information required for tissue extension.

Tissue hollowing and lumen formation

Many organs and embryos change their topology through the formation of fluid-filled lumens. This process occurs in organs such as the liver canaliculi, the otic vesicle or blastocyst formation in the early mouse embryo and is regulated by mechanics, hydraulics and cell and tissue geometry^{170–176}.

Fluid-filled lumens form within the extracellular space of simple cell aggregates (FIG. 6a) either by apoptosis in the centre of the aggregate or through the polarized secretion of fluid-filled vesicles^{177,178}. Lumen growth is powered by water flux through cells owing to a gradient of osmotic pressure maintained by energy-consuming ion pumps that drive polarized ion transport inside the lumen^{173,179–182}. The hydrostatic pressure within the lumen is resisted by cortical tension in the surrounding

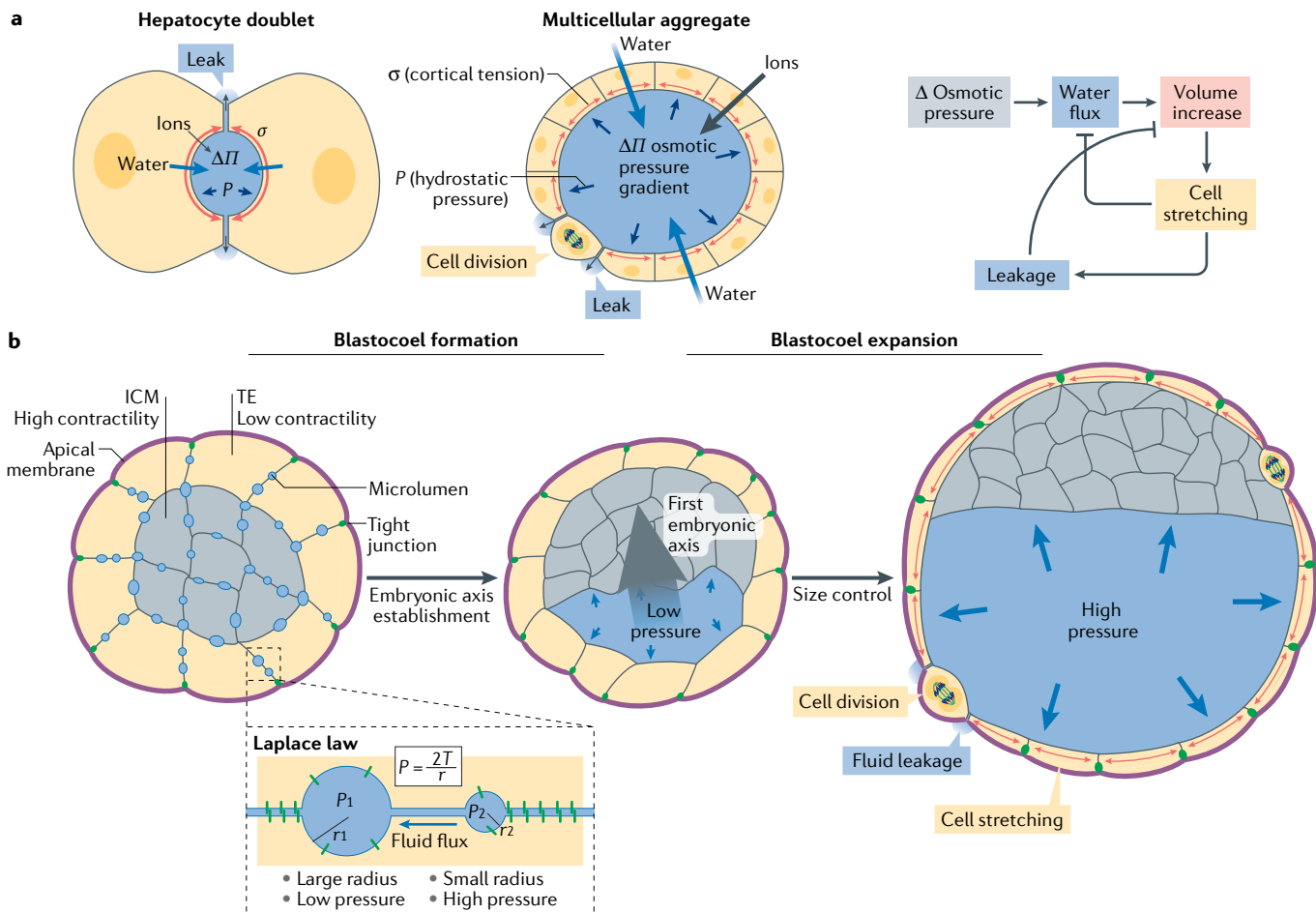


Fig. 6 | Mechanical and geometrical feedbacks control lumen formation to regulate tissue size and patterning. **a |** Schematics illustrating the process of lumen formation and growth in cell doublets, for example, doublets of liver cells (hepatocytes) surrounding bile canaliculi (on the left), and in multicellular aggregates (middle). In both cases water flux (inward-facing blue arrows) is driven by the difference (Δ) in osmotic pressure (Π) between the lumen and the surrounding cells. Active ion transport (black arrows) by pumps such as Na^+/K^+ ATPases fuels the osmotic pressure difference ($\Delta\Pi$). The hydrostatic pressure P (blue outward-facing arrows) stretches the surrounding cells and is resisted by cortical tension σ (bidirectional red arrows). The lumen grows in size up to a point of equilibrium established by negative feedbacks either due to fluid leakage through cell-cell junctions (represented by leakage through short junctions

in cell doublets or through junctions weakened by cell divisions in cell aggregates) or by reduced water flux. **b |** Illustration of the process of blastocoel formation and expansion in mouse blastocysts. The formation of a fluid-filled cavity begins with the formation of hundreds of microlumens (left), which discharge their fluid to a single larger cavity owing to a difference in Laplace pressure, where P is pressure and T is tension (inset). The green small lines in the inset indicate E-cadherin molecules. The single larger cavity forms invariantly between the trophectoderm (TE) cells and the inner cell mass (ICM), setting the first embryonic axis. Successively the blastocoel cavity grows by water influx, causing stretching and increasing mechanical tension in TE cells, which continues up to the point of size equilibrium established by fluid leakage during cell division in the TE.

tissue^{175,177} (FIG. 6a). Small lumens are unstable, but once they reach a critical size they grow, powered by the osmotic pressure difference. A negative feedback explains how lumen size reaches a stable steady state or oscillatory dynamics around a fixed size. The spherical nature of the lumen-surrounding tissue is such that surface tension increases as the hydrostatic pressure of the growing lumen increases. When the tension increases, cells stretch and, above a certain threshold, water may leak through cell–cell junctions, leading to water efflux. In result, the lumen shrinks rapidly as documented in organoids and the mouse blastocyst^{174,176}. Water influx may also be reduced in response to the increase of internal pressure building up with increased fluid accumulation, as documented in the zebrafish otic vesicle¹⁸³. Finally, lumen dynamics may reflect competition between active ion transport, water flux, passive ion permeation, cortical tension and leakage through junctions, which depends on the geometry of the cell aggregate as shown for liver canaliculi¹⁷⁵. Thus, lumen formation and growth are governed by many feedbacks and follow principles of self-organization.

In some cases, lumen formation and growth also control the patterning and size of an organ or an embryo, as in the formation and growth of the blastocoel in the mouse embryo. The blastocyst is the mammalian pre-implantation embryo composed of the trophectoderm (TE), an extra-embryonic tissue that envelopes the inner cell mass (ICM) forming the embryo proper, and a fluid-filled lumen termed blastocoel. The blastocoel is positioned invariantly at the interface between TE and the ICM, the latter clustering on one side, thus breaking the initial radial symmetry of the embryo. This initial polarization sets the first embryonic axis, which later defines the main axis of the mammalian body¹⁸⁴. Blastocoel formation in mouse embryos begins with the simultaneous accumulation of fluid in hundreds of micrometre-sized lumens in the intercellular space between cell–cell contacts in blastomeres¹⁸⁵ (FIG. 6b). A rise in intercellular hydrostatic pressure locally ‘fractures’ E-cadherin cell–cell junctions and forms these microlumens. As the microlumens are connected, the fluid eventually converges in a single large lumen by flowing from small to large lumens owing to pressure differences and periluminal contractility. Patterning cell–cell adhesion and cell contractility orients the fluid flow and defines the final position of the blastocoel¹⁸⁵. Although there are no known patterns of cell–cell adhesion molecules in the mouse blastocyst, ICM and TE cells have different cortical tension. Higher contractility in ICM cells drives their initial internalization in the embryo^{186,187}. The blastocoel forms at the interface between the highly contractile ICM cells and the softer surrounding TE cells, which maintain a polarized structure with an apical plasma membrane domain at the cell-free interface (FIG. 6b). In TE cells the presence of an apical plasma membrane domain reduces actomyosin contractility^{186,188}, such that cell contractility depends on the cells’ position within the embryo. Thus, mechanical and geometrical information position the blastocoel and set the first embryonic axis in mouse embryos.

Epiblast

Also known as primitive ectoderm. One of two distinct layers arising from the inner cell mass in the mammalian blastocyst or the blastodisc in avian and reptile embryos. In mammals, the epiblast sits between the trophectoderm and the hypoblast (or primitive endoderm).

Primitive endoderm

Also known as hypoblast. One of two layers arising from the inner cell mass in the mammalian blastocyst. The primitive endoderm sits between the epiblast and the blastocoel.

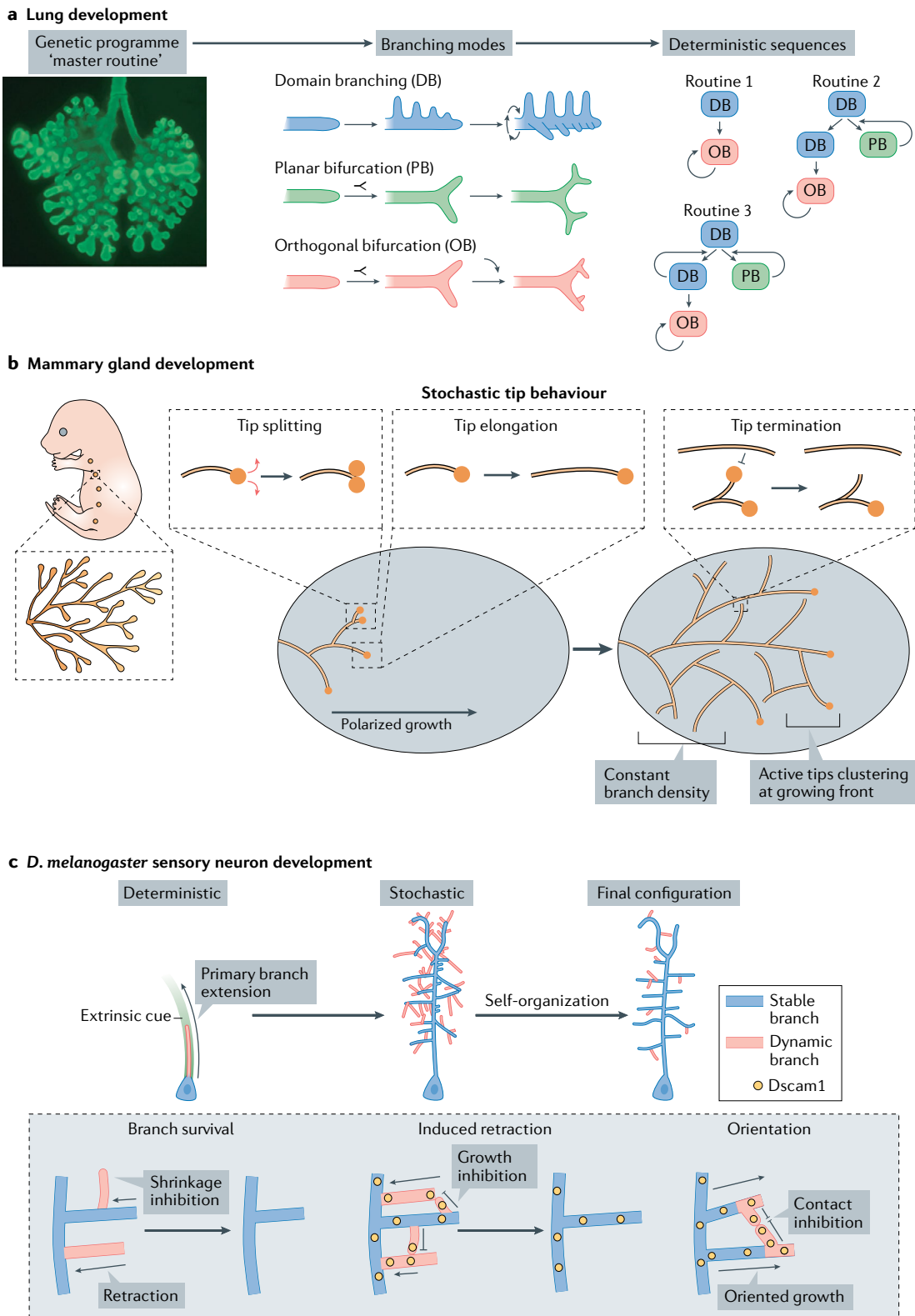
Once formed and positioned, the blastocoel keeps accumulating fluid, ultimately enlarging the blastocyst. The swelling of the blastocoel is resisted by tight junctions, which prevent fluid leakage, and by cortical tension of TE cells (FIG. 6b). The expansion of the blastocoel stretches TE cells, which in turn respond by increasing their contractility and strengthening tight junctions by a mechanical feedback¹⁷⁶. The blastocyst keeps increasing its size up to a threshold in cortical tension when it starts to undergo reversible collapse events due to loss of tight junction integrity when TE cells divide. Thus, feedback between lumen pressure, cell contractility and junction stability regulate the size of the embryo in a self-organized manner¹⁷⁶. Regulation of the lumen size affects in turn cell fate specification within the embryo. Decreasing the size of the lumen decreases stretching in the cells surrounding the cavity and thus facilitates their internalization possibly by affecting their division. Indeed, less stretched cells may more easily orient their axis of division radially, leading to a higher number of asymmetrical divisions, with one cell inheriting the apical domain and remaining in the outer layer, and the other cell losing the apical domain and distributing towards the centre of the cell mass. As the loss of an apical surface is required to downregulate CDX2 (REFS^{189,190}) — a TE cell fate determinant — thereby driving the ICM fate, regulation of blastocyst size also impacts on specification of blastocyst cell identities¹⁷⁶. Furthermore, the expansion of the blastocoel, through a mechanism not yet fully characterized but involving the secretion of FGF-coated vesicles in the fluid-filled lumen, also patterns the spatial segregation of the epiblast and primitive endoderm cells within the ICM¹⁹¹. Thus, mechanical and geometrical cues set size and patterning in the blastocyst through the regulation of biochemical signalling.

Altogether, hydrostatic pressure drives tissue morphogenesis, and mechanical as well as geometrical feedback mechanisms control tissue size and patterning. This provides an example of self-organized tissue morphogenesis in the absence of a pre-established genetic programme.

Branching morphogenesis

Branched structures are ubiquitous in nature, from molecules to cells and entire organs. Many internal organs, such as the pulmonary tract, exocrine glands, the kidney and the vascular system, have branched structures that are essential for their functions. Excellent reviews^{192–194} summarize the known molecular mechanisms of morphogenesis of branched organs; here, we illustrate how branching morphogenesis follows the principles of programmed morphogenesis or self-organization.

The *D. melanogaster* tracheal system is a highly ramified epithelial tubular network that transports oxygen to internal organs. Its branching pattern is highly stereotyped¹⁹⁵ and is driven by sources of FGF (encoded by *branchless* (*bnl*) in *D. melanogaster*) as a guidance cue¹⁹⁶. Tracheal development begins with the invagination of 20 epithelial sacs, each sprouting finer branches to generate a tree-like structure. Sprouting depends on the migratory activity of a few epithelial cells towards a



localized source of FGF¹⁹⁶. The expression pattern of the FGF source is not fixed but changes dynamically. Once the first branches reach the source of FGF, *bnl* expression is turned off and branches stop growing. Successively, expression of *bnl* at a new location guides branch elongation towards the new patch¹⁹⁶. Thus, the localized and dynamic expression of a source of FGF signalling

controls deterministically the branching pattern, as in a programme.

The development of the mouse lung also shows stereotypical patterns akin to a programme. The reconstruction of the complete branching history of the pulmonary tree identified three unique and geometrically simple modes of branching that form the entire pulmonary

Fig. 7 | Morphogenesis of branched structures can be genetically programmed or emerge as self-organized. **a** | On the left, an image of a developing mouse lung. In the middle, a representation of the three stereotyped modes of branching observed during development of the airways in mouse lungs. On the right, a schematic illustrating the three deterministic sequences (routines) of execution of the branching modes during the development of the branched network. Mouse lung development has been proposed to be directed by a genetically encoded ‘master routine’, which deterministically defines which branching mode is executed at each position in the tree according to the specific routine that is being followed. **b** | Development of the branched ductal network of a mammary gland in mouse. Active tips, that is, the region where cell proliferation is active and drives expansion of the ductal network, undergo stochastically one of the three behaviours illustrated in the insets: they can bifurcate, giving rise to two active tips; they can proliferate, elongating the ductal tube; or they can terminate when they encounter a maturing duct. The specific dynamic features of the developing branched network—constant branch density and active tips clustering at the growing front—emerge from the ensemble of these stochastic behaviours of the active tips. **c** | Cartoon illustration of the development of dendritic arborization in vpda class I neurons in *D. melanogaster*. The extension of the primary dendritic branch is deterministic and follows hypothetical patterned extrinsic cues (in green). Then, sprouting and stabilization of the secondary and tertiary branches occurs stochastically and follows principles of self-organization. The grey box depicts three local behaviours that occur stochastically and define the stabilization or retraction of secondary and tertiary branches. On the left the growth of a new tertiary branch (small rounded-tip branch in red) prevents the shrinkage of the parent secondary branch beyond the branch point (branch stabilization). In the middle, new Dscam1 (a cell adhesion molecule inducing contact-mediated retraction)-positive branches (small rounded-tip red branches) contact pre-existing branches (red flat-end branches) and inhibit their growth to induce their retraction (induced retraction). On the right, the contact-induced inhibition between two daughter branches (small rounded-tip red branches) orients the growth of the two parent branches. Image in part **a** reprinted from REF.¹⁹⁷, Springer Nature Limited. Middle diagram in part **a** adapted from REF.¹⁹⁷, Springer Nature Limited. Schematic in part **c** reprinted with permission from REF.²⁰⁴, Elsevier.

tree¹⁹⁷ (FIG. 7a). These three branching modes do not occur randomly in the lineage but follow one of three possible specific sequences (FIG. 7a). Thus, like a programme, individual modules (the branching modes) are repeated according to deterministic routines (the branching sequences), proposed to be genetically encoded by a master routine¹⁹⁷, the nature of which remains to be determined.

Contrasting with the evidence for programmed morphogenesis of branches, it was proposed that the morphogenesis of branched organs (for example, the mouse mammary gland and kidney) can also emerge from stochastic rules for the branching, elongation and termination of the tips of the network¹⁹⁸ (FIG. 7b). Key features of the branched network could be predicted by a model in which the branch tips can either bifurcate or elongate in a random direction with equal probability and terminate when they reach the proximity of existing ducts, thereby introducing a density-dependent negative feedback on network growth. In this case, the precise shape of the network is not predetermined genetically but self-organized as it emerges from a space-filling strategy driven by local rules and feedback. This model predicted several features of the branched trees in the mouse mammary gland and kidney such as a structural heterogeneity of network subtrees and a constant density of branches, and it demonstrated that in-built polarity of network growth can emerge without any chemotactic gradient¹⁹⁸ (FIG. 7b). This study shows how branching can be self-organized through local interactions and feedbacks. In this case, the global network topology and its features are defined by statistical rules of intrinsically noisy cell dynamics.

PVD neurons

Sensory neurons responding to harsh touch and cold temperatures with a highly elaborate dendritic arborization in the nematode *Caenorhabditis elegans*.

Vpda class I neurons

Sensory neurons of the peripheral nervous system of *Drosophila melanogaster* embryos and larvae. The classification is based on the morphology of the dendritic arborization with class I being the simplest morphology and class IV the most complex.

The dichotomy between programme and self-organization is not limited to the branching of multicellular internal organs. Single neurons also display features of deterministic and self-organized branching in growing their dendritic arborizations. One context in which deterministic rules fully determine the arborization pattern are the dendrites of the PVD neurons in *C. elegans*. Very stereotypical dendrite arborizations are established in PVD neurons during postembryonic development^{199,200} and are dependent on patterned cues provided in the epidermis^{201–203}. Here, the ligand complex SAX-7-L1CAM-MNR-1 expressed in the skin controls the growth of ‘menorah’-like dendrites by acting as a short-range cue for branching points^{201,202}. In *D. melanogaster* the shape of the dendritic arborization in vpda class I neurons is defined by a combination of deterministic rules and self-organization (FIG. 7c). In these neurons, the growth of the primary branch occurs very robustly in a predetermined direction, whereas the secondary and tertiary branches display fluctuations in length and number characteristic of stochastic systems²⁰⁴. Live imaging of dendritic growth and computational modelling revealed that the shape of the neuronal arborization emerges from a few local statistical rules of branch dynamics. Moreover, the tree geometry exerts a constant feedback on local branch dynamics in two opposite ways: ‘parent’ branch stabilization by ‘daughter’ branches and contact-induced self-repulsion of internal branches²⁰⁴. Thus, the morphogenesis of complex branched dendritic arborizations rests on both deterministic and self-organizational principles.

Conclusions and perspectives

What drives the emergence of reproducible biological forms? The information that underlies morphogenesis is inherited genetically. However, even though genes organize — via their biochemical products and downstream signalling — cell biological processes in space and time, they do not do it explicitly, and it is essential to consider the physical environment in which they operate. Understanding how genes encode shape requires a characterization of fundamental physical properties of living matter that are not genetically encoded, but emerge as a consequence of cell form and function. Such properties can be encapsulated in specific parameters of theoretical models, for instance, the law of diffusion, the theory of linear elasticity and active matter theory, that explain how dynamics emerge from local out-of-equilibrium properties of molecules or cells. Biochemistry and mechanics both define length and timescales and as such underlie how shapes emerge. Morphogenetic information is thus inherently mechano-chemical.

Morphogenetic information is also geometrical. Geometry of a tissue defines the system’s boundary conditions, impacts on local stress patterns and can reshape chemical gradients. This has profound consequences on how mechano-chemical information is deployed in space and time. Although geometry provides essential information to guide morphogenesis, cells cannot directly sense geometrical cues, but do so only via stresses and biochemical activities that arise from geometry. Thus, shapes and geometry sensing emerge from

mechano-chemical information, and in turn geometry may feed back and modulate local molecular activity and local mechanics. As such, the morphogenetic information is recursive as it acts upon itself and constantly changes through feedback. We addressed this in the context of tissue invagination and folding, tissue extension, tissue hollowing and tissue branching. We argue that similar principles apply more generally to other morphogenetic processes such as tissue zippering, which occurs in many developmental contexts. A striking example of this is illustrated during neural tube closure in the urochordate *Ciona robusta*. In this system, tissue zippering relies on a wave of junction contraction driven by MyoII contractility followed by junction relaxation. Zippering emerges from the dynamic interplay between patterns of cadherin expression, the geometry of cell-cell contacts and the mechanics of actomyosin contraction. Contraction deforms cell contacts, changes tissue geometry locally and thereby transmits information to reiterate the cycle in a more anterior group of cells^{205,206}.

We delineated two idealized and distinct modalities of information flow during morphogenesis. Programmes specify deterministically and hierarchically all operations required for the development of a shape. Programmed morphogenesis results explicitly and predictably from the spatially organized initial conditions, a pre-pattern, and relies upon deterministic rules. For instance, a genetically encoded morphogen gradient specifies a battery of downstream decisions that themselves dictate mechanical states in cells such as cell contractility. By contrast, self-organization is characterized by the emergence of ordered structures from a purely homogeneous initial state. It relies on stochastic rules, local activity associated with molecular motors and dissipation of elastic energy, driving irreversible deformation and amplification of local activity via feedbacks that operate across scales. Thereby, the system transits to a steady state that minimizes its free energy.

Programmed and self-organized processes differ in several other ways that will be important to address rigorously in the future. First, the amount of information required to specify each process appears different. In programmes, all steps need to be specified deterministically, and a large number of parameters are tuned. By contrast, self-organized dynamics rely on very sparse information such as differential growth rates and elastic properties during buckling, differential diffusivity in Turing instabilities or differential surface tension. A simple quantitative difference in a physical parameter can produce an instability leading to an equilibrium or steady-state shape. Second, programme and self-organization exhibit differences in robustness, translating to differences in resistance to internal (that is, genetic)

or external perturbations. Programmes are usually hard-wired and exhibit redundancy, such that they are mostly insensitive to genetic perturbations. However, once affected, for example by a mutation, they cannot be repaired to generate the expected shape because of the absence of feedbacks and a strict dependency on initial conditions, which may be lost as morphogenesis proceeds. By contrast, owing to their internal feedbacks, rapid dynamics and insensitivity to initial conditions, self-organized systems can reform after complete perturbations and constantly adapt to a changing environment. Thus, programmes may be most suited to robustly guide a few critical steps of morphogenesis where failing to properly time or position singular shape changes of the tissue may affect the entire subsequent steps of the morphogenesis, such as during embryo gastrulation or the specification of primary sulci in the developing brain cortex. However, for processes for which the large number and position of deformations need not be specified precisely (for example, feather buds or gut villi), self-organization may be better suited as the final pattern can emerge from a few specified parameters stochastically. Moreover, self-organized morphogenesis is associated with repair and regeneration capacity: this is the case for the mammary gland and gut villi for instance. The development of organoids in recent years builds upon this principle.

Finally, it is important to emphasize that these two modes of information flow are idealized strategies that, as we have seen above, always seem to coexist, although one may prevail over the other in specific morphogenetic processes or during a given phase of morphogenesis. Often the result of a self-organized process produces an initial asymmetry that programmes subsequent events. In embryos for instance, the initial asymmetry of the egg is usually self-organized (for example, at fertilization, which can occur at random locations), yet the resulting polarized determinants programme subsequent cellular decisions (as seen in *C. elegans* for example²⁰⁷). Conversely, asymmetries that result from embryo patterning can elicit mechanical processes that subsequently propagate in a self-organized manner^{43,205}.

The time seems ripe to consider the new ways in which shapes dynamically emerge during development. Looking at the nature and flow of morphogenetic information as we propose in this Review provides a powerful framework for tackling how shapes emerge during development but also how they may evolve. Indeed, the space of possible shapes is structured by morphogenetic information and as such is not strictly governed by genes but also by mechanics and geometry.

Published online 22 January 2021

- Waddington, C. H. *The Strategy of the Genes: a Discussion of Some Aspects of Theoretical Biology* (George Allen and Unwin, London, 1957).
- Slack, J. M. Conrad Hal Waddington: the last renaissance biologist? *Nat. Rev. Genet.* **3**, 889–895 (2002).
- Roux, W. in *Foundations of Experimental Embryology* (eds Willier, B. H. & Oppenheimer, J. M.) 2–37 (Hafner, 1888).
- De Robertis, E. M. Spemann's organizer and self-regulation in amphibian embryos. *Nat. Rev. Mol. Cell Biol.* **7**, 296–302 (2006).
- Sulston, J. E., Schierenberg, E., White, J. G. & Thomson, J. N. The embryonic cell lineage of the nematode *Caenorhabditis elegans*. *Dev. Biol.* **100**, 64–119 (1983).
- Maduro, M. F. Cell fate specification in the *C. elegans* embryo. *Dev. Dyn.* **239**, 1315–1329 (2010).
- Nishida, H. & Stach, T. Cell lineages and fate maps in tunicates: conservation and modification. *Zool. Sci.* **31**, 645–652 (2014).
- Garcia-Bellido, A. & Santamaría, P. Developmental analysis of the wing disc in the mutant engrailed of *Drosophila melanogaster*. *Genetics* **72**, 87–104 (1972).
- Pradel, J. & White, R. A. From selectors to realizers. *Int. J. Dev. Biol.* **42**, 417–421 (1998).
- Halder, G., Callaerts, P. & Gehring, W. J. Induction of ectopic eyes by targeted expression of the eyeless gene in *Drosophila*. *Science* **267**, 1788–1792 (1995).
- Halder, G., Callaerts, P. & Gehring, W. J. New perspectives on eye evolution. *Curr. Opin. Genet. Dev.* **5**, 602–609 (1995).

12. Chanut-Delalande, H., Fernandes, I., Roch, F., Payre, F. & Plaza, S. Shavenbaby couples patterning to epidermal cell shape control. *PLoS Biol.* **4**, e290 (2006).
13. Driesch, H. The potency of the first two cleavage cells in echinoderm development: experimental production of double and partial formation. Reprinted in *Foundations of Experimental Embryology* (eds Willier, B. H. & Oppenheimer, J. M.) (Hafner, 1892).
14. Morgan, T. H. Half-embryos and whole-embryos from one of the first two blastomeres of the frog's egg. *Anat. Anz.* **10**, 623–628 (1895).
15. Spemann, H. *Embryonic Development and Induction*, Vol. 10 (Taylor & Francis, 1988).
16. Browne, E. N. The production of new hydranths in Hydra by the insertion of small grafts. *J. Exp. Zool.* **7**, 1–23 (1909).
17. Spemann, H. & Mangold, H. Induction of embryonic primordia by implantation of organizers from a different species. *Roux Arch. Entwickl. Mech.* **100**, 599–638 (1924).
18. Gilmour, D., Rembold, M. & Leptin, M. From morphogen to morphogenesis and back. *Nature* **541**, 311–320 (2017).
19. Hannezo, E. & Heisenberg, C. P. Mechanochemical feedback loops in development and disease. *Cell* **178**, 12–25 (2019).
20. Schweisguth, F. & Corson, F. Self-organization in pattern formation. *Dev. Cell* **49**, 659–677 (2019).
21. Turing, A. M. The chemical basis of morphogenesis. *Philos. Trans. R. Soc. London. Ser. B, Biol. Sci.* **237**, 37–72 (1952).
22. Prusinkiewicz, P., Meinhardt, H. & Fowler, D. R. *The Algorithmic Beauty of Sea Shells* (Springer, 2003).
23. Gelets, L., Anderson, G. A. & Ferrell, J. E. Jr. Spatial trigger waves: positive feedback gets you a long way. *Mol. Biol. Cell* **25**, 3486–3493 (2014).
24. Wartlick, O. et al. Dynamics of Dpp signaling and proliferation control. *Science* **331**, 1154–1159 (2011).
25. Rogers, K. W. & Schier, A. F. Morphogen gradients: from generation to interpretation. *Annu. Rev. Cell Dev. Biol.* **27**, 377–407 (2011).
26. Sagner, A. & Briscoe, J. Morphogen interpretation: concentration, time, competence, and signaling dynamics. *Wiley Interdiscip. Rev. Dev. Biol.* **6**, e271 (2017).
27. Economou, A. D. et al. Periodic stripe formation by a Turing mechanism operating at growth zones in the mammalian palate. *Nat. Genet.* **44**, 348–351 (2012).
28. Sheth, R. et al. Hox genes regulate digit patterning by controlling the wavelength of a Turing-type mechanism. *Science* **338**, 1476–1480 (2012).
29. Pourquié, O. The segmentation clock: converting embryonic time into spatial pattern. *Science* **301**, 328–330 (2003).
30. Mayer, M., Depken, M., Bois, J. S., Julicher, F. & Grill, S. W. Anisotropies in cortical tension reveal the physical basis of polarizing cortical flows. *Nature* **467**, 617–621 (2010).
31. Clement, R., Dehapont, B., Collinet, C., Lecuit, T. & Lenne, P. F. Viscoelastic dissipation stabilizes cell shape changes during tissue morphogenesis. *Curr. Biol.* **27**, 3132–3142 e3134 (2017).
32. Dasbiswas, K., Hannezo, E. & Gov, N. S. Theory of epithelial cell shape transitions induced by mechanoactive chemical gradients. *Biophys. J.* **114**, 968–977 (2018).
33. Dicko, M. et al. Geometry can provide long-range mechanical guidance for embryogenesis. *PLoS Comput. Biol.* **13**, e1005443 (2017).
34. Oster, G. F., Murray, J. D. & Harris, A. K. Mechanical aspects of mesenchymal morphogenesis. *J. Embryol. Exp. Morphol.* **78**, 83–125 (1983).
35. Shyer, A. E. et al. Emergent cellular self-organization and mechanosensation initiate follicle pattern in the avian skin. *Science* **357**, 811–815 (2017).
36. Hannezo, E., Dong, B., Recho, P., Joanny, J. F. & Hayashi, S. Cortical instability drives periodic supracellular actin pattern formation in epithelial tubes. *Proc. Natl. Acad. Sci. USA* **112**, 8620–8625 (2015).
37. Ladoux, B., Nelson, W. J., Yan, J. & Mège, R. M. The mechanotransduction machinery at work at adherens junctions. *Integr. Biol.* **7**, 1109–1119 (2015).
38. Collinet, C. & Lecuit, T. Stability and dynamics of cell-cell junctions. *Prog. Mol. Biol. Transl. Sci.* **116**, 25–47 (2013).
39. Papusheva, E. & Heisenberg, C.-P. Spatial organization of adhesion: force-dependent regulation and function in tissue morphogenesis. *EMBO J.* **29**, 2753–2768 (2010).
40. Schwayer, C. et al. Mechanosensation of tight junctions depends on ZO-1 phase separation and flow. *Cell* **179**, 937–952 e918 (2019).
41. Lecuit, T., Lenne, P. F. & Munro, E. Force generation, transmission, and integration during cell and tissue morphogenesis. *Annu. Rev. Cell Dev. Biol.* **27**, 157–184 (2011).
42. Geiger, B., Spatz, J. P. & Bershadsky, A. D. Environmental sensing through focal adhesions. *Nat. Rev. Mol. Cell Biol.* **10**, 21–33 (2009).
43. Bailles, A. et al. Genetic induction and mechanochemical propagation of a morphogenetic wave. *Nature* **572**, 467–473 (2019). **Shows that a mechano-chemical wave of Rho1–MyoII activation drives invagination and anterior movement of the posterior endoderm during *D. melanogaster* gastrulation. It shows the relevance of self-organized contractile waves in driving tissue invagination and movements.**
44. Kindberg, A., Hu, J. K. & Bush, J. O. Forced to communicate: integration of mechanical and biochemical signaling in morphogenesis. *Curr. Opin. Cell Biol.* **66**, 59–68 (2020).
45. Munjal, A., Philippe, J. M., Munro, E. & Lecuit, T. A self-organized biomechanical network drives shape changes during tissue morphogenesis. *Nature* **524**, 351–355 (2015). **Shows how pulsed contractility during *D. melanogaster* germband extension depends on self-organizational properties of actomyosin networks, that is, an advection-mediated positive feedback on MyoII activation due to the association of Rho1GTP, Rho to actomyosin cortex.**
46. Goehring, N. W. et al. Polarization of PAR proteins by advective triggering of a pattern-forming system. *Science* **334**, 1137–1141 (2011).
47. Michaux, J. B., Robin, F. B., McFadden, W. M. & Munro, E. M. Excitable RhoA dynamics drive pulsed contractions in the early *C. elegans* embryo. *J. Cell Biol.* **217**, 4230–4252 (2018).
48. Durdu, S. et al. Luminal signalling links cell communication to tissue architecture during organogenesis. *Nature* **515**, 120–124 (2014).
49. Shyer, A. E., Huycke, T. R., Lee, C., Mahadevan, L. & Tabin, C. J. Bending gradients: how the intestinal stem cell gets its home. *Cell* **161**, 569–580 (2015). **Shows that mechanical buckling of intestinal villi in chick and mouse embryos distorts a chemical gradient of SHH and restricts stem cell proliferation at the villus base. It shows the relevance of tissue geometry in shaping the morphogenetic information.**
50. Martin, A. C. & Goldstein, B. Apical constriction: themes and variations on a cellular mechanism driving morphogenesis. *Development* **141**, 1987–1998 (2014).
51. Munjal, A. & Lecuit, T. Actomyosin networks and tissue morphogenesis. *Development* **141**, 1789–1793 (2014).
52. Leptin, M. & Grunewald, B. Cell shape changes during gastrulation in *Drosophila*. *Development* **110**, 73–84 (1990).
53. Sweeton, D., Parks, S., Costa, M. & Wieschaus, E. Gastrulation in *Drosophila*: the formation of the ventral furrow and posterior midgut invaginations. *Development* **112**, 775–789 (1991).
54. Martin, A. C., Kaschube, M. & Wieschaus, E. F. Pulsed contractions of an actin–myosin network drive apical constriction. *Nature* **457**, 495–499 (2009). **Shows that cell apical constriction during invagination of the mesoderm in *D. melanogaster* is driven by medio-apical actomyosin pulsed contractions instead of purse-string contractility at adherens junctions as previously thought.**
55. Gelbart, M. A. et al. Volume conservation principle involved in cell lengthening and nucleus movement during tissue morphogenesis. *Proc. Natl. Acad. Sci. USA* **109**, 19298–19303 (2012).
56. Krueger, D., Tardivo, P., Nguyen, C. & De Renzis, S. Downregulation of basal myosin-II is required for cell shape changes and tissue invagination. *EMBO J.* **37**, e100170, <https://doi.org/10.15252/embj.2018100170> (2018).
57. Gracia, M. et al. Mechanical impact of epithelial–mesenchymal transition on epithelial morphogenesis in *Drosophila*. *Nat. Commun.* **10**, 2951 (2019).
58. Sherrard, K., Robin, F., Lemaire, P. & Munro, E. Sequential activation of apical and basolateral contractility drives ascidian endoderm invagination. *Curr. Biol.* **20**, 1499–1510 (2010). **Identifies a two-step mechanism for endoderm invagination in ascidian embryos: first, a Rho1–**
- ROCK–MyoII-mediated phase of cell apical constriction and second, a phase of apico-basal shortening dependent on MyoII but not on Rho1–ROCK. It shows the relevance of polarized actomyosin contractility in driving 3D cell shape changes during invagination.**
59. Mason, F. M., Tworoger, M. & Martin, A. C. Apical domain polarization localizes actin–myosin activity to drive ratchet-like apical constriction. *Nat. Cell Biol.* **15**, 926–936 (2013).
60. Vasquez, C. G., Tworoger, M. & Martin, A. C. Dynamic myosin phosphorylation regulates contractile pulses and tissue integrity during epithelial morphogenesis. *J. Cell Biol.* **206**, 435–450 (2014).
61. Izquierdo, E., Quirkin, T. & De Renzis, S. Guided morphogenesis through optogenetic activation of Rho signalling during early *Drosophila* embryogenesis. *Nat. Commun.* **9**, 2366 (2018).
62. Reeves, G. T. & Stathopoulos, A. Graded dorsal and differential gene regulation in the *Drosophila* embryo. *Cold Spring Harb. Perspect. Biol.* **1**, a000836 (2009).
63. Manning, A. J., Peters, K. A., Peifer, M. & Rogers, S. L. Regulation of epithelial morphogenesis by the G protein-coupled receptor mist and its ligand fog. *Sci. Signal.* **6**, ra98 (2013).
64. Costa, M., Wilson, E. T. & Wieschaus, E. A putative cell signal encoded by the folded gastrulation gene coordinates cell shape changes during *Drosophila* gastrulation. *Cell* **76**, 1075–1089 (1994).
65. Kolsch, V., Seher, T., Fernandez-Ballester, G. J., Serrano, L. & Leptin, M. Control of *Drosophila* gastrulation by apical localization of adherens junctions and RhoGEF2. *Science* **315**, 384–386 (2007).
66. Lee, J. Y. et al. Wnt/Frizzled signaling controls *C. elegans* gastrulation by activating actomyosin contractility. *Curr. Biol.* **16**, 1986–1997 (2006).
67. Roh-Johnson, M. et al. Triggering a cell shape change by exploiting preexisting actomyosin contractions. *Science* **335**, 1232–1235 (2012).
68. Marston, D. J. et al. MRCK-1 drives apical constriction in *C. elegans* by linking developmental patterning to force generation. *Curr. Biol.* **26**, 2079–2089 (2016).
69. Nishimura, T. & Takeichi, M. Shroom3-mediated recruitment of Rho kinases to the apical cell junctions regulates epithelial and neuroepithelial planar remodeling. *Development* **135**, 1493–1502 (2008).
70. Haigo, S. L., Hildebrand, J. D., Harland, R. M. & Wallingford, J. B. Shroom induces apical constriction and is required for hinge point formation during neural tube closure. *Curr. Biol.* **13**, 2125–2137 (2003).
71. Chung, M. I., Nascone-Yoder, N. M., Grover, S. A., Drysdale, T. A. & Wallingford, J. B. Direct activation of Shroom3 transcription by Pitx proteins drives epithelial morphogenesis in the developing gut. *Development* **137**, 1339–1349 (2010).
72. Plageman, T. F. Jr. et al. Pax6-dependent Shroom3 expression regulates apical constriction during lens placode invagination. *Development* **137**, 405–415 (2010).
73. Plageman, T. F. Jr. et al. A Trio-RhoA-Shroom3 pathway is required for apical constriction and epithelial invagination. *Development* **138**, 5177–5188 (2011).
74. Ernst, S. et al. Shroom3 is required downstream of FGF signalling to mediate proneuroblast assembly in zebrafish. *Development* **139**, 4571–4581 (2012).
75. Hildebrand, J. D. Shroom regulates epithelial cell shape via the apical positioning of an actomyosin network. *J. Cell Sci.* **118**, 5191–5203 (2005).
76. Lang, R. A., Herman, K., Reynolds, A. B., Hildebrand, J. D. & Plageman, T. F. Jr. p120-catenin-dependent junctional recruitment of Shroom3 is required for apical constriction during lens pit morphogenesis. *Development* **141**, 3177–3187 (2014).
77. Rauzi, M., Lenne, P. F. & Lecuit, T. Planar polarized actomyosin contractile flows control epithelial junction remodelling. *Nature* **468**, 1110–1114 (2010).
78. Solon, J., Kaya-Copur, A., Colombelli, J. & Brunner, D. Pulised forces timed by a ratchet-like mechanism drive directed tissue movement during dorsal closure. *Cell* **137**, 1331–1342 (2009).
79. Munro, E., Nance, J. & Piress, J. R. Cortical flows powered by asymmetrical contraction transport PAR proteins to establish and maintain anterior-posterior polarity in the early *C. elegans* embryo. *Dev. Cell* **7**, 413–424 (2004).
80. Kim, H. Y. & Davidson, L. A. Punctuated actin contractions during convergent extension and their permissive regulation by the non-canonical Wnt-signaling pathway. *J. Cell Sci.* **124**, 635–646 (2011).

81. Maitre, J. L., Niwayama, R., Turlier, H., Nedelec, F. & Hiiragi, T. Pulsatile cell-autonomous contractility drives compaction in the mouse embryo. *Nat. Cell Biol.* **17**, 849–855 (2015).
82. Xie, S. & Martin, A. C. Intracellular signalling and intercellular coupling coordinate heterogeneous contractile events to facilitate tissue folding. *Nat. Commun.* **6**, 7161 (2015).
83. Yevick, H. G., Miller, P. W., Dunkel, J. & Martin, A. C. Structural redundancy in supracellular actomyosin networks enables robust tissue folding. *Dev. Cell* **50**, 586–598 e583 (2019).
84. Bhide, S. et al. Mechanical competition alters the cellular interpretation of an endogenous genetic programme. Preprint at *bioRxiv* <https://doi.org/10.1101/2020.10.15.333963> (2020).
85. Odell, G. M., Oster, G., Alberch, P. & Burnside, B. The mechanical basis of morphogenesis. I. Epithelial folding and invagination. *Dev. Biol.* **85**, 446–462 (1981).
86. Llinàres-Benadero, C. & Borrell, V. Deconstructing cortical folding: genetic, cellular and mechanical determinants. *Nat. Rev. Neurosci.* **20**, 161–176 (2019).
87. Garcia, K. E., Kroenke, C. D. & Bayly, P. V. Mechanics of cortical folding: stress, growth and stability. *Philos. Trans. R. Soc. Lond. B Biol. Sci.* **373**, 20170321 (2018).
88. Huycke, T. R. & Tabin, C. J. Chick midgut morphogenesis. *Int. J. Dev. Biol.* **62**, 109–119 (2018).
89. Walton, K. D., Mishkind, D., Riddle, M. R., Tabin, C. J. & Gumucio, D. L. Blueprint for an intestinal villus: species-specific assembly required. *Wiley Interdiscip. Rev. Dev. Biol.* **7**, e517 (2018).
90. Vasung, L. et al. Quantitative and qualitative analysis of transient fetal compartments during prenatal human brain development. *Front. Neuroanat.* **10**, 11 (2016).
91. Neal, J. et al. Insights into the gyration of developing ferret brain by magnetic resonance imaging. *J. Anat.* **210**, 66–77 (2007).
92. Lohmann, G., von Cramon, D. Y. & Colchester, A. C. Deep sulcal landmarks provide an organizing framework for human cortical folding. *Cereb. Cortex* **18**, 1415–1420 (2008).
93. Ono, M., Kubik, S. & Abernathy, C. D. *Atlas of the Cerebral Sulci* (G. Thieme Verlag, 1990).
94. Mota, B. & Herculano-Houzel, S. Cortical folding scales universally with surface area and thickness, not number of neurons. *Science* **349**, 74–77 (2015).
95. Van Essen, D. C. A tension-based theory of morphogenesis and compact wiring in the central nervous system. *Nature* **385**, 313–318 (1997).
96. Lefèvre, J. & Mangin, J. F. A reaction-diffusion model of human brain development. *PLoS Comput. Biol.* **6**, e1000749 (2010).
97. Richman, D. P., Stewart, R. M., Hutchinson, J. W. & Caviness, V. S. Jr. Mechanical model of brain convolutional development. *Science* **189**, 18–21 (1975).
98. Hannezo, E., Prost, J. & Joanny, J. F. Instabilities of monolayered epithelia: shape and structure of villi and crypts. *Phys. Rev. Lett.* **107**, 078104 (2011).
99. Ben Amar, M. & Jia, F. Anisotropic growth shapes intestinal tissues during embryogenesis. *Proc. Natl. Acad. Sci. USA* **110**, 10525–10530 (2013).
100. Mahadevan, L. & Rica, S. Self-organized origami. *Science* **307**, 1740 (2005).
101. Xu, G. et al. Axons pull on the brain, but tension does not drive cortical folding. *J. Biomech. Eng.* **132**, 071013 (2010).
102. Tallinen, T., Chung, J. Y., Biggins, J. S. & Mahadevan, L. Gyration from constrained cortical expansion. *Proc. Natl. Acad. Sci. USA* **111**, 12667–12672 (2014).
103. Tallinen, T. et al. On the growth and form of cortical convolutions. *Nat. Phys.* **12**, 588–593 (2016). Shows that the initial size and geometry of the structure coupled with mechanical instability due to differential tangential growth accounts for the cortical folding pattern observed in fetal human brains. It shows the importance of the initial geometry in positioning folds.
104. Kriegstein, A., Noctor, S. & Martinez-Cerdeno, V. Patterns of neural stem and progenitor cell division may underlie evolutionary cortical expansion. *Nat. Rev. Neurosci.* **7**, 883–890 (2006).
105. Smart, I. H., Dehay, C., Giroud, P., Berland, M. & Kennedy, H. Unique morphological features of the proliferative zones and postmitotic compartments of the neural epithelium giving rise to striate and extrastriate cortex in the monkey. *Cereb. Cortex* **12**, 37–53 (2002).
106. Reillo, I., de Juan Romero, C., García-Cabezas, M. A. & Borrell, V. A role for intermediate radial glia in the tangential expansion of the mammalian cerebral cortex. *Cereb. Cortex* **21**, 1674–1694 (2011).
107. de Juan Romero, C., Bruder, C., Tomasello, U., Sanz-Angueta, J. M. & Borrell, V. Discrete domains of gene expression in germinal layers distinguish the development of gyrencephaly. *EMBO J.* **34**, 1859–1874 (2015).
108. Savin, T. et al. On the growth and form of the gut. *Nature* **476**, 57–62 (2011). Shows that gut looping arises from growth differences between the gut tube and the anchoring dorsal mesenteric sheet. It documents that equilibrium linear elasticity theory accounts for complex tissue geometry *in vivo*.
109. Lyons, K. M., Pelton, R. W. & Hogan, B. L. Organogenesis and pattern formation in the mouse: RNA distribution patterns suggest a role for bone morphogenetic protein-2A (BMP-2A). *Development* **109**, 835–844 (1990).
110. Nerurkar, N. L., Mahadevan, L. & Tabin, C. J. BMP signaling controls buckling forces to modulate looping morphogenesis of the gut. *Proc. Natl. Acad. Sci. USA* **114**, 2277–2282 (2017).
111. Coulombre, A. J. & Coulombre, J. L. Intestinal development. I. Morphogenesis of the villi and musculature. *J. Embryol. Exp. Morphol.* **6**, 403–411 (1958).
112. Shyer, A. E. et al. Villification: how the gut gets its villi. *Science* **342**, 212–218 (2013). Shows that the different steps of avian gut villification result from a mechanical instability due to the expansion of the growing endoderm and the constraints imposed by surrounding muscle layers.
113. Grey, R. D. Morphogenesis of intestinal villi. I. Scanning electron microscopy of the duodenal epithelium of the developing chick embryo. *J. Morphol.* **137**, 193–213 (1972).
114. Burgess, D. R. Morphogenesis of intestinal villi. II. Mechanism of formation of previous ridges. *J. Embryol. Exp. Morphol.* **34**, 723–740 (1975).
115. Walton, K. D., Freddo, A. M., Wang, S. & Gumucio, D. L. Generation of intestinal surface: an absorbing tale. *Development* **143**, 2261–2272 (2016).
116. Walton, K. D. et al. Villification in the mouse: Bmp signals control intestinal villus patterning. *Development* **143**, 427–436 (2016).
117. Harris, A. K., Stopak, D. & Warner, P. Generation of spatially periodic patterns by a mechanical instability: a mechanical alternative to the Turing model. *J. Embryol. Exp. Morphol.* **80**, 1–20 (1984).
118. Devonport, D. Tissue morphodynamics: translating planar polarity cues into polarized cell behaviors. *Semin. Cell Dev. Biol.* **55**, 99–110 (2016).
119. Shindo, A. Models of convergent extension during morphogenesis. *Wiley Interdiscip. Rev. Dev. Biol.* **7**, e293 (2018).
120. Huebner, R. J. & Wallingford, J. B. Coming to consensus: a unifying model emerges for convergent extension. *Dev. Cell* **46**, 389–396 (2018).
121. Keller, R. & Tibbetts, P. Mediolateral cell intercalation in the dorsal, axial mesoderm of *Xenopus laevis*. *Dev. Biol.* **131**, 539–549 (1989).
122. Wilson, P. & Keller, R. Cell rearrangement during gastrulation of *Xenopus*: direct observation of cultured explants. *Development* **112**, 289–300 (1991).
123. Shih, J. & Keller, R. Patterns of cell motility in the organizer and dorsal mesoderm of *Xenopus laevis*. *Development* **116**, 915–930 (1992).
124. Shih, J. & Keller, R. Cell motility driving mediolateral intercalation in explants of *Xenopus laevis*. *Development* **116**, 901–914 (1992).
125. Davidson, L. A., Marsden, M., Keller, R. & Desimone, D. W. Integrin $\alpha_5\beta_1$ and fibronectin regulate polarized cell protrusions required for *Xenopus* convergence and extension. *Curr. Biol.* **16**, 833–844 (2006).
126. Skoglund, P., Rolo, A., Chen, X., Gumbiner, B. M. & Keller, R. Convergence and extension at gastrulation require a myosin IIB-dependent cortical actin network. *Development* **135**, 2435–2444 (2008).
127. Munro, E. M. & Odell, G. M. Polarized basolateral cell motility underlies invagination and convergent extension of the ascidian notochord. *Development* **129**, 13–24 (2002).
128. Williams-Masson, E. M., Heid, P. J., Lavin, C. A. & Hardin, J. The cellular mechanism of epithelial rearrangement during morphogenesis of the *Caenorhabditis elegans* dorsal hypodermis. *Dev. Biol.* **204**, 263–276 (1998).
129. Walck-Shannon, E., Reiner, D. & Hardin, J. Polarized Rac-dependent protrusions drive epithelial intercalation in the embryonic epidermis of *C. elegans*. *Development* **142**, 3549–3560 (2015).
130. Sun, Z. et al. Basolateral protrusion and apical contraction cooperatively drive *Drosophila* germ-band extension. *Nat. Cell Biol.* **19**, 375–383 (2017).
131. Williams, M., Yen, W., Lu, X. & Sutherland, A. Distinct apical and basolateral mechanisms drive planar cell polarity-dependent convergent extension of the mouse neural plate. *Dev. Cell* **29**, 34–46 (2014).
132. Irvine, K. D. & Wieschaus, E. Cell intercalation during *Drosophila* germband extension and its regulation by pair-rule segmentation genes. *Development* **120**, 827–841 (1994).
133. Bertet, C., Sulak, L. & Lecuit, T. Myosin-dependent junction remodelling controls planar cell intercalation and axis elongation. *Nature* **429**, 667–671 (2004).
134. Blankenship, J. T., Backovic, S. T., Sanny, J. S., Weitz, O. & Zallen, J. A. Multicellular rosette formation links planar cell polarity to tissue morphogenesis. *Dev. Cell* **11**, 459–470 (2006). Together with Bertet et al. (2004), shows that cell intercalation during germband extension in *D. melanogaster* is due to a planar polarized process of cell-cell contact remodelling in which MyoII accumulates at shrinking junctions.
135. Fernandez-Gonzalez, R. & Zallen, J. A. Oscillatory behaviors and hierarchical assembly of contractile structures in intercalating cells. *Phys. Biol.* **8**, 045005 (2011).
136. Collinet, C., Rauzi, M., Lenne, P. F. & Lecuit, T. Local and tissue-scale forces drive oriented junction growth during tissue extension. *Nat. Cell Biol.* **17**, 1247–1258 (2015).
137. Yu, J. C. & Fernandez-Gonzalez, R. Local mechanical forces promote polarized junctional assembly and axis elongation in *Drosophila*. *eLife* **5**, e10757 (2016).
138. Rauzi, M., Verant, P., Lecuit, T. & Lenne, P. F. Nature and anisotropy of cortical forces orienting *Drosophila* tissue morphogenesis. *Nat. Cell Biol.* **10**, 1401–1410 (2008).
139. Fernandez-Gonzalez, R., Simoes Sde, M., Roper, J. C., Eaton, S. & Zallen, J. A. Myosin II dynamics are regulated by tension in intercalating cells. *Dev. Cell* **17**, 736–743 (2009).
140. Bambadekar, K., Clement, R., Blanc, O., Chardes, C. & Lenne, P. F. Direct laser manipulation reveals the mechanics of cell contacts *in vivo*. *Proc. Natl. Acad. Sci. USA* **112**, 1416–1421 (2015).
141. Kale, G. R. et al. Distinct contributions of tensile and shear stress on E-cadherin levels during morphogenesis. *Nat. Commun.* **9**, 5021 (2018).
142. Roznicki, E. et al. Myosin-II-mediated cell shape changes and cell intercalation contribute to primitive streak formation. *Nat. Cell Biol.* **17**, 397–408 (2015).
143. Nishimura, T., Honda, H. & Takeichi, M. Planar cell polarity links axes of spatial dynamics in neural-tube closure. *Cell* **149**, 1084–1097 (2012).
144. Shindo, A. & Wallingford, J. B. PCP and sepinin compartmentalize cortical actomyosin to direct collective cell movement. *Science* **343**, 649–652 (2014).
145. Shindo, A., Inoue, Y., Kinoshita, M. & Wallingford, J. B. PCP-dependent transcellular regulation of actomyosin oscillation facilitates convergent extension of vertebrate tissue. *Dev. Biol.* **446**, 159–167 (2019).
146. Zallen, J. A. & Wieschaus, E. Patterned gene expression directs bipolar planar polarity in *Drosophila*. *Dev. Cell* **6**, 343–355 (2004).
147. Pare, A. C. et al. A positional Toll receptor code directs convergent extension in *Drosophila*. *Nature* **515**, 523–527 (2014). Identifies three Toll receptors as downstream targets of pair-rule genes that direct planar polarization in cells of *D. melanogaster* germband.
148. Lavallou, J. et al. Formation of mechanical interfaces by self-organized Toll-8/Cirr GPCR asymmetry. Preprint at *bioRxiv* <https://doi.org/10.1101/2020.03.16.993758> (2020).
149. Wallingford, J. B. Planar cell polarity and the developmental control of cell behavior in vertebrate embryos. *Annu. Rev. Cell Dev. Biol.* **28**, 627–653 (2012).
150. Yang, Y. & Mlodzik, M. Wnt-Frizzled/planar cell polarity signaling: cellular orientation by facing the wind (Wnt). *Annu. Rev. Cell Dev. Biol.* **31**, 623–646 (2015).
151. Butler, M. T. & Wallingford, J. B. Planar cell polarity in development and disease. *Nat. Rev. Mol. Cell Biol.* **18**, 375–388 (2017).

152. Strutt, D. I., Weber, U. & Mlodzik, M. The role of RhoA in tissue polarity and Frizzled signalling. *Nature* **387**, 292–295 (1997).
153. Winter, C. G. et al. Drosophila Rho-associated kinase (Drok) links Frizzled-mediated planar cell polarity signaling to the actin cytoskeleton. *Cell* **105**, 81–91 (2001).
154. Andreeva, A. et al. PTK7-Src signaling at epithelial cell contacts mediates spatial organization of actomyosin and planar cell polarity. *Dev. Cell* **29**, 20–33 (2014).
155. Habas, R., Dawid, I. B. & He, X. Coactivation of Rac and Rho by Wnt/Frizzled signaling is required for vertebrate gastrulation. *Genes Dev.* **17**, 295–309 (2003).
156. Heisenberg, C. P. et al. Silberblick/Wnt11 mediates convergent extension movements during zebrafish gastrulation. *Nature* **405**, 76–81 (2000).
157. Wallingford, J. B. et al. Dishevelled controls cell polarity during Xenopus gastrulation. *Nature* **405**, 81–85 (2000).
158. Keys, D. N., Levine, M., Harland, R. M. & Wallingford, J. B. Control of intercalation is cell-autonomous in the notochord of *Ciona intestinalis*. *Dev. Biol.* **246**, 329–340 (2002).
159. Butler, M. T. & Wallingford, J. B. Spatial and temporal analysis of PCP protein dynamics during neural tube closure. *eLife* **7**, e36456 (2018).
160. Habas, R., Kato, Y. & He, X. Wnt/Frizzled activation of Rho regulates vertebrate gastrulation and requires a novel Formin homology protein Daam1. *Cell* **107**, 843–854 (2001).
161. Kim, S. K. et al. Planar cell polarity acts through septins to control collective cell movement and ciliogenesis. *Science* **329**, 1337–1340 (2010).
162. Levayer, R. & Lecuit, T. Oscillation and polarity of E-cadherin asymmetries control actomyosin flow patterns during morphogenesis. *Dev. Cell* **26**, 162–175 (2013).
163. Lye, C. M. et al. Mechanical coupling between endoderm invagination and axis extension in Drosophila. *PLoS Biol.* **13**, e1002292 (2015).
164. Saadaoui, M., Rocancourt, D., Roussel, J., Corson, F. & Gros, J. A tensile ring drives tissue flows to shape the gastrulating amniote embryo. *Science* **367**, 453–458 (2020).
165. Aigouy, B. et al. Cell flow reorients the axis of planar polarity in the wing epithelium of Drosophila. *Cell* **142**, 773–786 (2010). **Shows that contraction of the hinge region during morphogenesis of the wing in Drosophila mechanically directs cell flows and ultimately orients PCP in the blade region.**
166. Etournay, R. et al. Interplay of cell dynamics and epithelial tension during morphogenesis of the Drosophila pupal wing. *eLife* **4**, e07090 (2015).
167. Ray, R. P. et al. Patterned anchorage to the apical extracellular matrix defines tissue shape in the developing appendages of Drosophila. *Dev. Cell* **34**, 310–322 (2015).
168. Munster, S. et al. Attachment of the blastoderm to the vitelline envelope affects gastrulation of insects. *Nature* **568**, 395–399 (2019). **Shows that blastoderm attachment to the enveloping vitelline membrane orients cellular flows during gastrulation of the beetle *Tribolium castaneum*, similar to Bailes et al. (2019). Shows the relevance of tissue boundary conditions in directing tissue flows during morphogenesis.**
169. Sato, K. et al. Left-right asymmetric cell intercalation drives directional collective cell movement in epithelial morphogenesis. *Nat. Commun.* **6**, 10074 (2015).
170. Coulombe, A. J. The role of intraocular pressure in the development of the chick eye. II. Control of corneal size. *AMA Arch. Ophthalmol.* **57**, 250–253 (1957).
171. Desmond, M. E. & Jacobson, A. G. Embryonic brain enlargement requires cerebrospinal fluid pressure. *Dev. Biol.* **57**, 188–198 (1977).
172. Abbas, L. & Whitfield, T. T. Nkcc1 (Slc12a2) is required for the regulation of endolymph volume in the otic vesicle and swim bladder volume in the zebrafish larva. *Development* **136**, 2837–2848 (2009).
173. Navis, A., Marjoram, L. & Bagnat, M. Cfr controls lumen expansion and function of Kupffer's vesicle in zebrafish. *Development* **140**, 1703–1712 (2013).
174. Ruiz-Herrero, T., Alessandri, K., Gurchenkov, B. V., Nassoy, P. & Mahadevan, L. Organ size control via hydraulically gated oscillations. *Development* **144**, 4422–4427 (2017).
175. Dasgupta, S., Gupta, K., Zhang, Y., Viasnoff, V. & Prost, J. Physics of lumen growth. *Proc. Natl. Acad. Sci. USA* **115**, E4751–E4757 (2018). **Quantitatively analyses the contributions of osmotic pressure, cortical tension, cell-cell contact geometry and paracellular leak in the expansion of intercellular lumens.**
176. Chan, C. J. et al. Hydraulic control of mammalian embryo size and cell fate. *Nature* **571**, 112–116 (2019). **Shows that feedback between luminal pressure and cortical tension controls the expansion of the mouse blastocysts and affects cell fate specification.**
177. Bryant, D. M. & Mostov, K. E. From cells to organs: building polarized tissue. *Nat. Rev. Mol. Cell Biol.* **9**, 887–901 (2008).
178. Sigurbjornsdottir, S., Mathew, R. & Leptin, M. Molecular mechanisms of de novo lumen formation. *Nat. Rev. Mol. Cell Biol.* **15**, 665–676 (2014).
179. Sperber, I. Secretion of organic anions in the formation of urine and bile. *Pharmacol. Rev.* **11**, 109–134 (1959).
180. Boyer, J. L. Bile formation and secretion. *Compr. Physiol.* **3**, 1035–1078 (2013).
181. Navis, A. & Bagnat, M. Developing pressures: fluid forces driving morphogenesis. *Curr. Opin. Genet. Dev.* **32**, 24–30 (2015).
182. Navis, A. & Nelson, C. M. Pulling together: tissue-generated forces that drive lumen morphogenesis. *Semin. Cell Dev. Biol.* **55**, 139–147 (2016).
183. Mosaliganti, K. R. et al. Size control of the inner ear via hydraulic feedback. *eLife* **8**, e39596 (2019).
184. Takaoka, K. & Hamada, H. Cell fate decisions and axis determination in the early mouse embryo. *Development* **139**, 3–14 (2012).
185. Dumortier, J. G. et al. Hydraulic fracturing and active coarsening position the lumen of the mouse blastocyst. *Science* **365**, 465–468 (2019). **Illustrates how the formation of blastocoel and the first symmetry breaking event in the mouse embryo depend on a self-organized process of hydraulic fracturing of cell-cell contacts followed by contractility-directed coarsening of microlumens.**
186. Maitre, J. L. et al. Asymmetric division of contractile domains couples cell positioning and fate specification. *Nature* **536**, 344–348 (2016).
187. Samarage, C. R. et al. Cortical tension allocates the first inner cells of the mammalian embryo. *Dev. Cell* **34**, 435–447 (2015).
188. Plusa, B. et al. Downregulation of Par3 and aPKC function directs cells towards the ICM in the preimplantation mouse embryo. *J. Cell Sci.* **118**, 505–515 (2005).
189. Nishioka, N. et al. The Hippo signaling pathway components Lats and Yap pattern Tead4 activity to distinguish mouse trophectoderm from inner cell mass. *Dev. Cell* **16**, 398–410 (2009).
190. Korotkevich, E. et al. The apical domain is required and sufficient for the first lineage segregation in the mouse embryo. *Dev. Cell* **40**, 235–247 e237 (2017).
191. Ryan, A. Q., Chan, C. J., Granner, F. & Hiiiragi, T. Lumen expansion facilitates epiblast-primitive endoderm fate specification during mouse blastocyst formation. *Dev. Cell* **51**, 684–697 e684 (2019).
192. Metzger, R. J. & Krasnow, M. A. Genetic control of branching morphogenesis. *Science* **284**, 1635–1639 (1999).
193. Affolter, M., Zeller, R. & Caussinus, E. Tissue remodelling through branching morphogenesis. *Nat. Rev. Mol. Cell Biol.* **10**, 831–842 (2009).
194. Ochoa-Espinosa, A. & Affolter, M. Branching morphogenesis: from cells to organs and back. *Cold Spring Harb. Perspect. Biol.* **4**, a008243, <https://doi.org/10.1101/cshperspect.a008243> (2012).
195. Affolter, M. & Caussinus, E. Tracheal branching morphogenesis in Drosophila: new insights into cell behaviour and organ architecture. *Development* **135**, 2055–2064 (2008).
196. Sutherland, D., Samakovlis, C. & Krasnow, M. A. branchless encodes a Drosophila FGF homolog that controls tracheal cell migration and the pattern of branching. *Cell* **87**, 1091–1101 (1996).
197. Metzger, R. J., Klein, O. D., Martin, G. R. & Krasnow, M. A. The branching programme of mouse lung development. *Nature* **453**, 745–750 (2008). **Reveals that the branching pattern of the mouse airways follows stereotypical patterns and sequences and suggests that it reflects the execution of a genetic programme instructing the morphogenesis of branched organs.**
198. Hanzeo, E. et al. A unifying theory of branching morphogenesis. *Cell* **171**, 242–255 e227 (2017). **Shows how the stochastic behaviour at the tips of a growing network accounts for several features of branching in the mouse mammary glands and kidney and the human prostate. It shows the relevance of self-organization in the morphogenesis of branched organs.**
199. Halevi, S. et al. The *C. elegans* ric-3 gene is required for maturation of nicotinic acetylcholine receptors. *EMBO J.* **21**, 1012–1020 (2002).
200. Tsalik, E. L. et al. LIM homeobox gene-dependent expression of biogenic amine receptors in restricted regions of the *C. elegans* nervous system. *Dev. Biol.* **263**, 81–102 (2003).
201. Dong, X., Liu, O. W., Howell, A. S. & Shen, K. An extracellular adhesion molecule complex patterns dendritic branching and morphogenesis. *Cell* **155**, 296–307 (2013).
202. Salzberg, Y. et al. Skin-derived cues control arborization of sensory dendrites in *Caenorhabditis elegans*. *Cell* **155**, 308–320 (2013).
203. Zou, W. et al. A multi-protein receptor-ligand complex underlies combinatorial dendrite guidance choices in *C. elegans*. *eLife* **5**, e18345 (2016).
204. Palavalli, A., Tizón-Escamilla, N., Rupprecht, J.-F. & Lecuit, T. Deterministic and stochastic rules of branching govern dendritic morphogenesis of sensory neurons. *Curr. Biol.* <https://doi.org/10.1016/j.cub.2020.10.054> (2020). **Shows that the morphogenesis of the dendritic arbour in a class of sensory neurons in *Drosophila* embryos results from a combination of deterministic events and self-organization.**
205. Hashimoto, H., Robin, F. B., Sherrard, K. M. & Munro, E. M. Sequential contraction and exchange of apical junctions drives zippering and neural tube closure in a simple chordate. *Dev. Cell* **32**, 241–255 (2015). **Shows that the process of neural tube closure in the chordate *Ciona robusta* depends on a self-organized cycle of MyoII contraction and neighbour exchange at the front of the zipping wave. Shows the relevance of self-organized processes in morphogenesis.**
206. Hashimoto, H. & Munro, E. Differential expression of a classic cadherin directs tissue-level contractile asymmetry during neural tube closure. *Dev. Cell* **51**, 158–172 e154 (2019).
207. Munro, E. & Bowerman, B. Cellular symmetry breaking during *Caenorhabditis elegans* development. *Cold Spring Harb. Perspect. Biol.* **1**, a003400 (2009).
208. Green, J. B. & Sharpe, J. Positional information and reaction-diffusion: two big ideas in developmental biology combine. *Development* **142**, 1203–1211 (2015).

Acknowledgements

The authors thank all members of the Lecuit group for stimulating discussions and useful feedback on this manuscript. This review emerged from a lecture series at the Collège de France in 2018. The lab is supported by the ERC grant SelfControl #788308 and the Ligue contre le Cancer. C.C. is supported by the CNRS and T.L. by the Collège de France.

Author contributions

The authors contributed equally to all aspects of the article.

Competing interests

The authors declare no competing interests.

Publisher's note

Springer Nature remains neutral with regard to jurisdictional claims in published maps and institutional affiliations.

© Springer Nature Limited 2021